BIOPHYSICS

Long-QT mutations in KCNE1 modulate the 17β-estradiol response of Kv7.1/KCNE1

Lisa-Marie Erlandsdotter[1], Lucilla Giammarino[2], Azemine Halili[1], Johan Nikesjö[1], Henrik Gréen[1,3], Katja E. Odening[2], Sara I. Liin[1]*

Estradiol (17β-E2) is implicated in higher arrhythmia risk of women with congenital or acquired long-QT syndrome (LQTS) compared to men. However, the underlying mechanisms remain poorly understood, and little is known about the impact of LQTS-associated mutations. We show that 17β-E2 inhibits the human cardiac Kv7.1/KCNE1 channel expressed in *Xenopus* oocytes. We find that the 17β-E2 effect depends on the Kv7.1 to KCNE1 stoichiometry, and we reveal a critical function of the KCNE1 carboxyl terminus for the effect. LQTS-associated mutations in the KCNE1 carboxyl terminus show a range of responses to 17β-E2, from a wild-type like response to impaired or abolished response. Together, this study increases our understanding of the mechanistic basis for 17β-E2 inhibition of Kv7.1/KCNE1 and demonstrates mutation-dependent responses to 17β-E2. These findings suggest that the 17β-E2 effect on Kv7.1/KCNE1 might contribute to the higher arrhythmia risk of women, particularly in carriers with specific LQTS-associated mutations.

INTRODUCTION

The cardiac action potential is the result of opening and closing/inactivation of ion channels, regulating the inward flow of depolarizing Na^+ and Ca^{2+} currents followed by the outward flow of repolarizing K^+ currents [reviewed in (*1*)]. The well-timed sequential conduction of different ionic currents is required for synchronized cardiomyocyte contraction and action potential propagation throughout the heart. Altered activity of any of the ion channels involved in the cardiac action potential may give rise to cardiac arrhythmias and, in the worst case, cause sudden cardiac death (SCD) (*1*, *2*). Long-QT syndrome (LQTS), characterized by a prolonged QT interval on the electrocardiogram, is one such potentially lethal arrhythmic disorder in which the prolonged action potential duration predisposes the ventricles to early afterdepolarizations, Torsade-de-Pointes ventricular arrhythmias, and SCD (*3*). Although LQTS is a relatively rare disorder [affecting about 1:2500 people (*4*)], its severity motivates studies aimed at understanding the mechanistic basis of LQTS.

Mutations in cardiac ion channels are the most common cause of congenital LQTS, of which mutations in the most abundantly affected genes encoding for the I_{Ks}, I_{Kr} (underlying the slow and rapid component of the delayed rectifier K^+ current, respectively), and Nav1.5 channels account together for about 90% of the cases (*5*). More than 300 mutations in the genes *KCNQ1* and *KCNE1*, encoding for the Kv7.1 α subunit and KCNE1 auxiliary subunit, respectively, of the I_{Ks} conducting channel, have been linked to congenital LQTS type 1 and 5 (i.e., LQT1 and LQT5) (*2*). In addition, there are acquired forms of LQTS caused by exogenous factors such as pharmaceutical drugs or endogenous modulators altering ion channel activity (*6*, *7*). Sex hormones are one class of endogenous modulators that has gained much attention as disease modulators of cardiac arrhythmias, with anticipated QT-shortening or QT-prolonging effects depending on hormone and targeted ion channel. In general, progesterone and testosterone are reported to have QT-shortening effects, mediated through inhibition of L-type voltage-gated Ca^{2+} (Cav) channels and activation of several cardiac Kv channels [reviewed in (*8*)]. In contrast, 17β-estradiol [17β-E2; the most abundant estrogen (*9*)] is, in general, considered to have QT-prolonging effects, mediated through activation of L-type Cav channels and inhibition of several cardiac Kv channels [reviewed in (*8*)]. The QT-shortening effect of testosterone in men and the QT-prolonging effect of 17β-E2 in women, which is partially counteracted by QT-shortening effects of progesterone, are hormonal influences likely to contribute to sex-related differences observed in the clinical phenotype of LQTS: Women have a longer heart rate–corrected QT interval than do men and are more prone to drug-induced LQTS (*10*), particularly during phases of the menstrual cycle with high 17β-E2 levels (*11*). Moreover, women with congenital LQTS show higher clinical penetrance and increased risk of life-threatening arrhythmic Torsade-de-Pointes events than men (*12*). Together, it is well established that sex hormones are clinically relevant modulators of cardiac ion channels. However, many aspects of how sex hormones modulate the activity of cardiac ion channels remain unknown, which limits a mechanistic understanding of beneficial and harmful effects and hampers personalized patient management. For instance, the I_{Ks} channel is composed of four Kv7.1 subunits and one to four KCNE1 subunits (*13*–*15*). Previous studies have observed a 17β-E2–mediated down-regulation of KCNE1 mRNA (*16*) that may reduce I_{Ks} currents, but little is known about channel properties or motifs required for 17β-E2 effects. Moreover, it remains to be determined whether LQTS-associated mutations modify the 17β-E2 effect. Characterizing the putative interplay between mutations implicated in congenital LQTS and sex hormone effects would be one step toward understanding which individuals are particularly susceptible to arrhythmia because of hormonal influences.

In this study, we aimed to expand the understanding of I_{Ks} channel properties or motifs important for 17β-E2 effects on I_{Ks}

[1]Department of Biomedical and Clinical Sciences, Linköping University, Linköping, Sweden. [2]Translational Cardiology, Department of Cardiology, Inselspital, University Hospital Bern and Department of Physiology, University of Bern, Bern, Switzerland. [3]Department of Forensic Genetics and Forensic Toxicology, National Board of Forensic Medicine, Linköping, Sweden.
*Corresponding author. Email: sara.liin@liu.se

current densities. To this end, we coexpressed human Kv7.1 and KCNE1 subunits in *Xenopus* oocytes to allow for the formation of I_{Ks} channels (hereafter referred to as Kv7.1/KCNE1) and studied the effect of 17β-E2 and other steroid sex hormones using two-electrode voltage clamp electrophysiology. We found that 17β-E2, but not the other tested steroid sex hormones, induced a prominent reduction of Kv7.1/KCNE1 currents. This reduction was dependent on the KCNE1 subunit and protein kinase C (PKC), with particular importance of the KCNE1 C terminus and conventional PKC isoforms (α, β, and/or γ). LQTS-associated mutations in KCNE1 altered the 17β-E2 effect. Moreover, we could demonstrate similar I_{Ks}-inhibitory 17β-E2 effects in mammalian cardiomyocytes and elucidated mechanisms that may account for differences in the concentrations of 17β-E2 needed to exhibit I_{Ks}-inhibiting effects in different experimental settings. Our study expands the understanding of how 17β-E2 modulates the Kv7.1/KCNE1 channel and suggests that the genetic background could tune arrhythmia susceptibility due to hormonal influences.

RESULTS

17β-E2 inhibits the Kv7.1/KCNE1 channel

The major steroid sex hormones encompass progesterone; testosterone; and the estrogens estrone, 17β-E2, and estriol. These hormones are synthesized from cholesterol and contain a common steroid backbone (i.e., three cyclohexane rings and one cyclopentane ring) and are distinguished by variability in the functional groups at carbon 3, 16, or/and 17 (Fig. 1A). We tested the effect of these sex hormones, at concentrations of 3 and 10 μM, on the human Kv7.1/KCNE1 channel expressed in *Xenopus laevis* oocytes. Hormone effects on the maximum conductance (G_{max}) and the voltage at which half-maximal conductance was achieved (V_{50}) were quantified to deduce hormone effects on overall current amplitude and the voltage dependence of the channel opening, respectively (see Material and Methods).

17β-E2 was the only hormone with significant effects on G_{max} (Fig. 1B). Concentrations of 3 and 10 μM 17β-E2 reduced G_{max} of Kv7.1/KCNE1 by −35 ± 6% and −58 ± 5%, respectively (Fig. 1, B and C, and table S1; $P < 0.0001$, see figures and tables for statistical details throughout this work). In contrast, G_{max} was unaffected by progesterone (representative example in Fig. 1D), testosterone, and estrogens estrone and estriol (Fig. 1B and table S1). Moreover, none of the hormones induced prominent shifts in V_{50}, which was shifted by a maximum of 5 mV (table S1). The onset of Kv7.1/KCNE1 current reduction induced by 17β-E2 was relatively rapid with effects achieved within 10 min (Fig. 1E). The washout of the 17β-E2 effect was slow and incomplete despite prolonged wash (>25 min) with control solution (Fig. 1E). The expected maximal 17β-E2 effect on G_{max} was −94% with a median inhibitory concentration (IC_{50}; i.e., the 17β-E2 concentration needed to cause 50% of the maximal effect) of 5.2 μM (Fig. 1F). Because of the 17β-E2–induced reduction in overall conductance without shifts in V_{50}, a similar extent of current reduction was observed at less depolarized voltages as exemplified for +40 mV in Fig. 1G (expected maximal 17β-E2 effect on $I_{40\ mV}$ was −95% with an IC_{50} of 5.3 μM). Together, in our experimental setting, 17β-E2 was the only hormone out of the five tested steroid sex hormones that reduced the current generated by the human Kv7.1/KCNE1 channel.

The 17β-E2 effect is KCNE1 dependent

We next tested whether the observed 17β-E2–mediated inhibition of Kv7.1/KCNE1 was KCNE1 dependent. 17β-E2 concentrations up to 100 μM did not affect G_{max} or V_{50} of Kv7.1 alone (ΔG_{max} and ΔV_{50} was within ±10% and ±1.6 mV, respectively; Fig. 2A and fig. S1A). To test whether Kv7.1/KCNE1-like gating is enough for 17β-E2 effects, we quantified the effect of 17β-E2 on the Kv7.1_F315A mutant, which gates in a Kv7.1/KCNE1-like manner (Fig. 2B) (*17*). Ten micromolar 17β-E2 had a small activating effect on Kv7.1_F351A (ΔG_{max} = +22 ± 5%, $n = 4$, $P = 0.02$ with one-sample *t* test; Fig. 2B), suggesting that the KCNE1 subunit itself is required for 17β-E2–mediated inhibition of the Kv7.1/KCNE1 channel. In line with a KCNE1 dependence of the 17β-E2 effect, reducing the number of KCNE1 subunits in the Kv7.1/KCNE1 complex also impaired the ability of 17β-E2 to reduce G_{max}. At subsaturating 17β-E2 concentrations, 17β-E2 induced a smaller effect on concatenated Kv7.1 and KCNE1 subunits promoting a 4:2 stoichiometry compared to coinjected Kv7.1/KCNE1, whereas the effect on concatemers promoting a 4:4 stoichiometry was comparable to that of coinjected Kv7.1/KCNE1 (fig. S1, B and C). Three micromolar 17β-E2 reduced G_{max} of concatemers promoting 4:2 stoichiometry by only −4 ± 2%, whereas G_{max} of concatemers promoting 4:4 stoichiometry was reduced by −22 ± 6% (fig. S1C). Ten micromolar 17β-E2 reduced G_{max} of concatemers promoting 4:2 stoichiometry by about half to that seen for concatemers promoting 4:4 stoichiometry (ΔG_{max} = −36 ± 6% compared to −60 ± 3%; fig. S1C). Thus, the KCNE1 subunit is required for 17β-E2 to reduce G_{max}, and the effect is tuned by the number of KCNE1 subunits.

Part of the KCNE1 C terminus is required for 17β-E2–mediated inhibition of Kv7.1/KCNE1

KCNE1 is a single-transmembrane helix protein of 129 amino acids with an extracellular N terminus, an intracellular C terminus, and a transmembrane portion encompassing approximately residues 46 to 66 (Fig. 2C) (*18*). Given the critical role of KCNE1 for 17β-E2 effects, we generated truncated KCNE1 variants with the aim to identify which region of the KCNE1 subunit is important for the 17β-E2 effect. We generated one N-terminal truncated (KCNE1_Δ2-38) and four C-terminal truncated (KCNE1_Δ67, KCNE1_Δ78, KCNE1_Δ80, and KCNE1_Δ102) KCNE1 variants (Fig. 2C; see table S5 for intrinsic biophysical properties of variants). The KCNE1_Δ78, KCNE1_Δ80, and KCNE1_Δ102 truncated variants responded to 17β-E2 comparable to WT Kv7.1/KCNE1 (Fig. 2D, fig. S2, and table S2). In contrast, the KCNE1_Δ2-38 and KCNE1_Δ67 truncated mutants responded with a significantly smaller reduction in G_{max} compared to WT Kv7.1/KCNE1 (Fig. 2D, fig. S2, and table S2). Ten micromolar 17β-E2 reduced G_{max} of Kv7.1/KCNE1_Δ2-38 by −26 ± 10%, whereas G_{max} of KCNE1_Δ67 was not reduced at all (ΔG_{max} was +2 ± 9%; Fig. 2D and table S2). For all truncated KCNE1 variants, ΔV_{50} in response to 17β-E2 remained within 7 mV (table S2). Together, these experiments suggest that several regions of KCNE1 influence the 17β-E2 effect. However, the lack of 17β-E2 effect on KCNE1_Δ67 and fully restored effect on KCNE1_Δ78 highlight a region encompassing residues 67 to 77 as of special interest for the 17β-E2 effect.

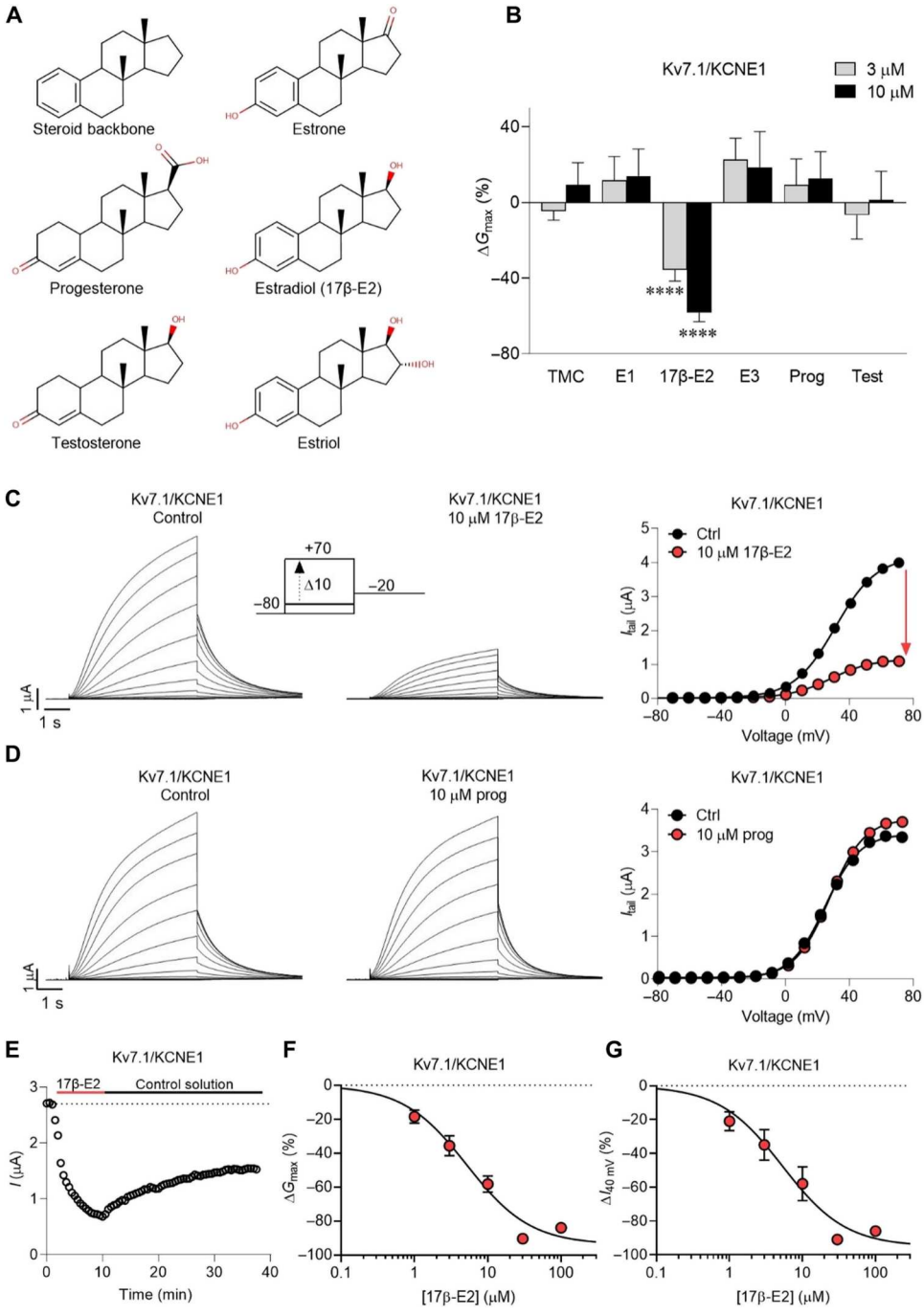

Fig. 1. 17β-E2 inhibits the Kv7.1/KCNE1 channel. (**A**) Molecular structure of the steroid backbone and indicated steroid sex hormones. (**B**) Summary of the effect of indicated concentrations of steroid sex hormones on G_{max} of Kv7.1/KCNE1. TMC, time-matched control (perfusion with control solution); E1, estrone; 17β-E2: estradiol; E3, estriol; Prog, progesterone; Test, testosterone. Data are shown as means ± SEM. n = 4 to 18 (table S1). Statistics indicate a one-sample t test compared to a hypothetical value of 0 (i.e., no change in G_{max}). ****$P < 0.0001$. $P > 0.05$ [not significant (n.s.)] for all other data (table S1). (**C**) Representative current family with corresponding $G(V)$ curve of Kv7.1/KCNE1 in the absence (left) and presence (middle) of 10 μM 17β-E2. Used voltage protocol is shown as inset. Curves in the $G(V)$ plot (right) represent Boltzmann fits (see Materials and Methods for details). For this specific cell, $V_{50,ctrl}$ = +31 mV, $I_{tailmax,ctrl}$ = 4.2 μA, $V_{50,17β\text{-}E2}$ = +28 mV, and $I_{tailmax,17β\text{-}E2}$ = 1.2 μA. (**D**) Same as in (C) but for progesterone. For this specific cell, $V_{50,ctrl}$ = +25 mV, $I_{tailmax,ctrl}$ = 3.4 μA, $V_{50,Prog}$ = +28 mV, and $I_{tailmax,Prog}$ = 3.8 μA. (**E**) Time course of onset/washout of 17β-E2 effect assessed by stepping to +40 mV from a holding voltage of −80 mV every 30 s (quantified at the end of the +40-mV pulse). Dashed line, current amplitude before 17β-E2 application. (**F**) Concentration dependence of the 17β-E2 effect on G_{max} of Kv7.1/KCNE1. See Materials and Methods for details of the concentration-response fit. Best fit, maximum ΔG_{max} = −94% and IC_{50} = 5.2 μM. Data are shown as means ± SEM. n = 4 to 18. Small error bars are covered by symbols. (**G**) Same as in (F) but for current amplitude at +40 mV. Best fit, maximum $\Delta I_{40\ mV}$ = −95% and IC_{50} = 5.3 μM.

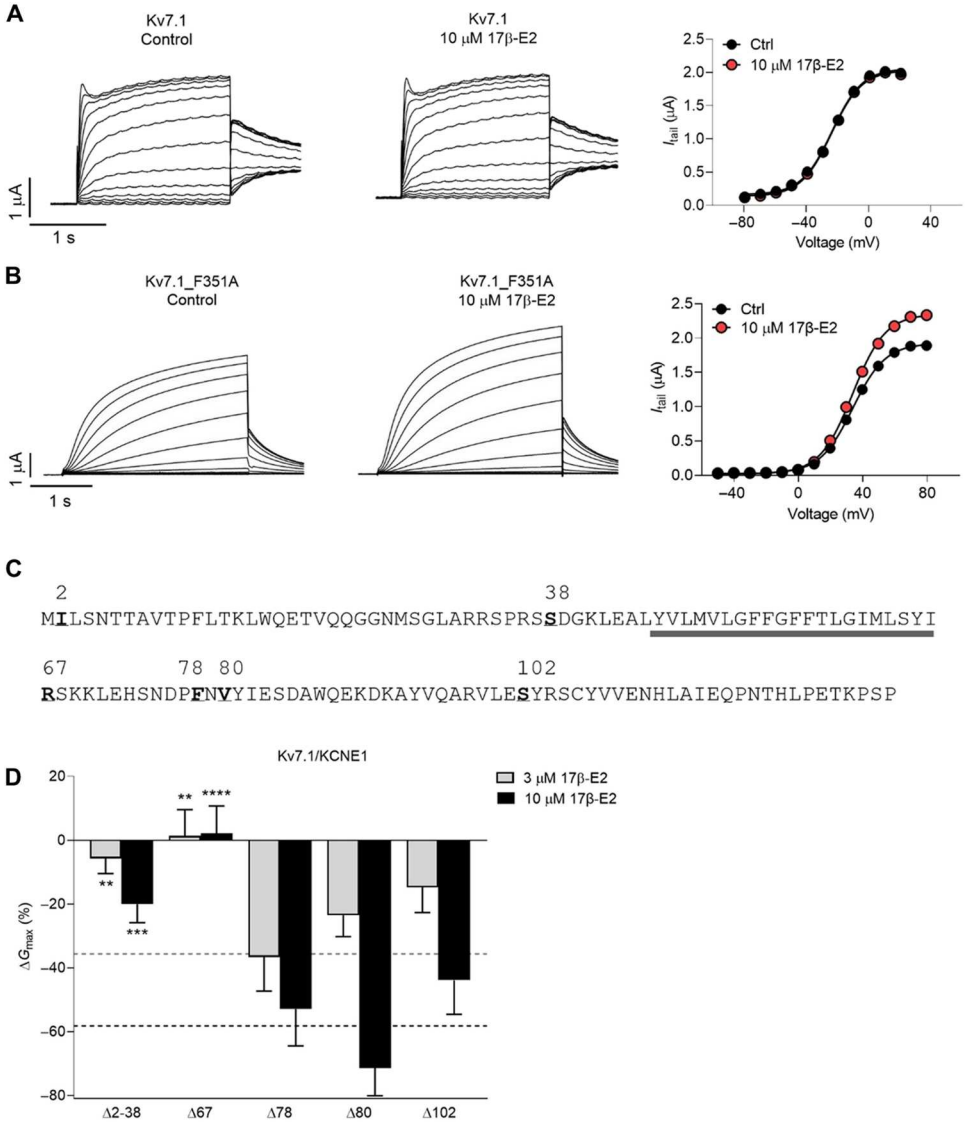

Fig. 2. 17β-E2 inhibition of Kv7.1/KCNE1 is KCNE1 dependent. (**A**) Representative current family with corresponding *G*(*V*) curve of Kv7.1 in the absence (left) and presence (middle) of 10 μM 17β-E2. Curves in the *G*(*V*) plot (right) represent Boltzmann fits. For this specific cell, $V_{50,ctrl}$ = −23 mV, $I_{tailmax,ctrl}$ = 2.1 μA, $V_{50,17β\text{-}E2}$ = −24 mV, and $I_{tailmax,17β\text{-}E2}$ = 2.0 μA. (**B**) Same as in (A) but for Kv7.1_F351A and 10 μM 17β-E2. For this specific cell, $V_{50,ctrl}$ = +34 mV, $I_{tailmax,ctrl}$ = 1.9 μA, $V_{50,17β\text{-}E2}$ = +34 mV, and $I_{tailmax,17β\text{-}E2}$ = 2.3 μA. (**C**) Amino acid sequence of KCNE1. Numbers indicate sites for truncations. Gray bar indicates the transmembrane portion of KCNE1. (**D**) Summary of the effect of 3 and 10 μM 17β-E2 on Kv7.1/KCNE1 channels with indicated KCNE1 truncations. Data are shown as means ± SEM. *n* = 4 to 13 (defined in table S2). Statistics indicate one-way analysis of variance (ANOVA) followed by Dunnett's multiple comparisons test to determine whether the 17β-E2 effect on truncated channels deviates from the effect on WT. ***P* < 0.01, ****P* < 0.001, and *****P* < 0.0001. *P* > 0.05 (n.s.) for all other data (see table S2). Gray and black dashed lines indicate the effect of 3 and 10 μM 17β-E2, respectively, on WT Kv7.1/KCNE1.

17β-E2–mediated inhibition of Kv7.1/KCNE1 is dependent on PKC

Steroid sex hormones such as 17β-E2 activate multiple signaling pathways (*19*). Rapid effects (obtained after several minutes or few hours) may be transduced via, for instance, membrane-bound classical steroid receptors (e.g., the estrogen receptors ERα and ERβ), nonclassical receptors such as G-protein–coupled receptors (e.g., GPR30), and protein kinases such as PKA and PKC (*19*–*21*). Slower signaling transduction, which typically has functional effects more than 6 hours after 17β-E2 treatment, may involve genomic pathways (*22*–*24*). 17β-E2–mediated inhibition of the Kv7.1/KCNE3 channel has been attributed to two underlying mechanisms involving PKC signaling: 17β-E2 has been proposed to reduce Kv7.1/KCNE3 membrane abundance by PKC-triggered dynamin-dependent channel internalization and to cause KCNE3 dissociation from Kv7.1 by stimulating PKC-mediated phosphorylation of S82 in KCNE3 (*25*–*27*). To evaluate the putative importance of PKC and other well-studied mediators involved in transducing rapid 17β-E2 effects, we used a set of receptor or kinase inhibitors (Fig. 3A, left), one by one, and assessed whether any of the inhibitors altered the reduction of G_{max} induced by 17β-E2 (see Materials

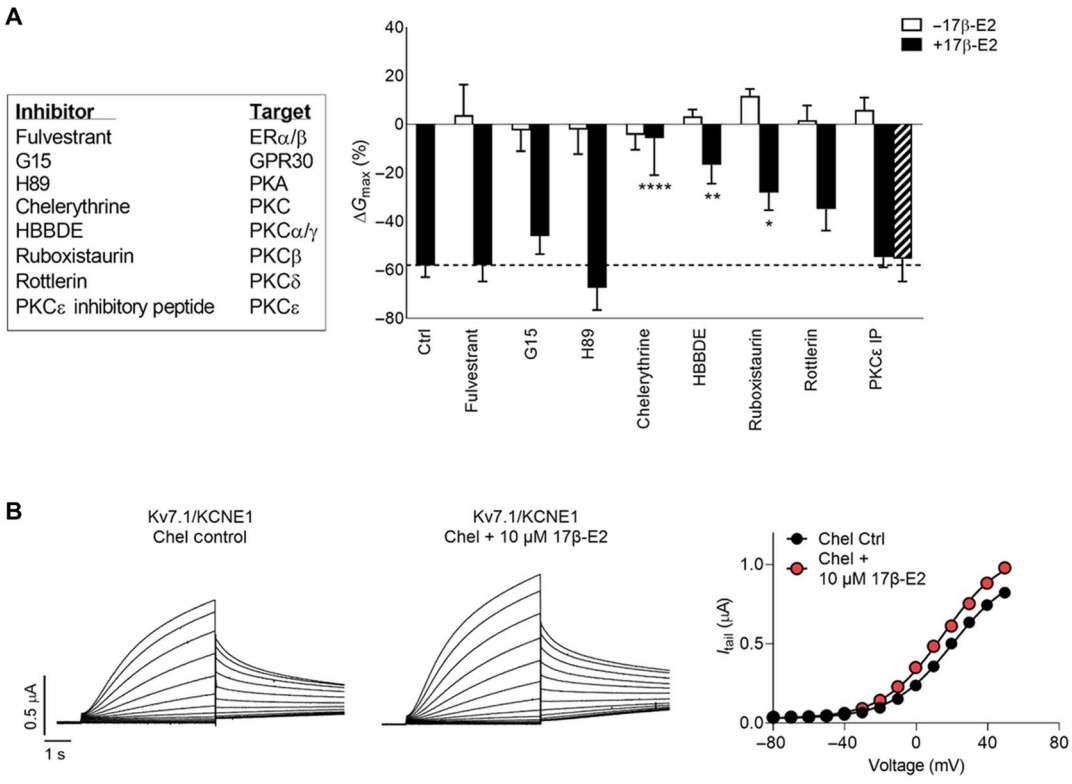

Fig. 3. 17β-E2 inhibition of Kv7.1/KCNE1 is PKC dependent. (**A**) Left: An overview of used receptor or kinase inhibitors with indicated primary target. Right: A summary of the effect of either control solution only (open bars, "−17β-E2") or 10 μM 17β-E2 (closed bars, "+17β-E2") on Kv7.1/KCNE1 exposed to indicated inhibitors (see Materials and Methods for details). The dashed bar for PKCε inhibitory peptide (IP) denotes data for oocytes injected with PKCε IP. Data are shown as means ± SEM. n = 3 to 9 (defined in table S3). Statistics indicate one-way ANOVA followed by Dunnett's multiple comparisons test to determine whether the 17β-E2 effect in the presence of inhibitors deviates from the effect on WT (included as bar marked "Ctrl"). *P < 0.05, **P < 0.01, and ****P < 0.0001. P > 0.05 (n.s.) for all other data (see table S3). (**B**) Representative current family with corresponding $G(V)$ curve of chelerythrine-treated Kv7.1/KCNE1 in the absence (left) and presence (middle) of 10 μM 17β-E2. Curves in the $G(V)$ plot (right) represent Boltzmann fits. For this specific cell, $V_{50,ctrl}$ = +20 mV, $I_{tailmax,ctrl}$ = 1.0 μA, $V_{50,17β\text{-}E2}$ = +15 mV, and $I_{tailmax,17β\text{-}E2}$ = 1.1 μA.

and Methods for concentrations and incubation times for the inhibitors).

Neither the ERα/ERβ antagonist fulvestrant nor the GPR30 antagonist G15 prevented 17β-E2 from reducing G_{max}. Ten micromolar 17β-E2 reduced G_{max} of Kv7.1/KCNE1 by −58 ± 7% in the presence of fulvestrant and −46 ± 7% in the presence of G15, compared with −58% in the absence of inhibitors (Fig. 3A and table S3). These data suggest that ER- and GPR30-mediated pathways are not involved in the 17β-E2 effect. The PKC antagonist chelerythrine, but not the PKA antagonist H89, abrogated the effect of 17β-E2 on G_{max}. Ten micromolar 17β-E2 reduced G_{max} of Kv7.1/KCNE1 by −67 ± 9% in the presence of H89 (Fig. 3A and table S3). In contrast, 10 μM 17β-E2 did not reduce G_{max} of Kv7.1/KCNE1 in the presence of chelerythrine (ΔG_{max} was −6 ± 15%; Fig. 3, A and B, and table S3). This suggests that the 17β-E2 effect is PKC, but not PKA, dependent.

X. laevis oocytes are known to express most types of PKCs (*28*) including the conventional PKCα, PKCβ, and PKCγ isoforms and novel PKCδ and PKCε isoforms. To further study the PKC dependence of the 17β-E2 effect, four PKC isotype–specific inhibitors were used: HBDDE (PKCα and PKCγ specific), ruboxistaurin (PKCβ specific), rottlerin (PKCδ specific), and PKCε inhibitor peptide (PKCε specific) (Fig. 3A). HBBDE and ruboxistaurin impaired the ability of 10 μM 17β-E2 to reduce G_{max} by about 50%, rendering a G_{max} reduction of −17 to −28% (Fig. 3A and table S3). Rottlerin and PKCε inhibitor peptide, however, did not significantly alter the ability of 10 μM 17β-E2 to reduce G_{max} (Fig. 3A and table S3). None of the inhibitors themselves significantly reduced G_{max} of Kv7.1/KCNE1 in the time range used to assess 17β-E2 effects (Fig. 3A, open bars, and table S3). However, ruboxistaurin alone significantly increased G_{max} of Kv7.1/KCNE1 by +12 ± 3% (Fig. 3A and table S3), indicating that the reduction in G_{max} induced by 17β-E2 in the ruboxistaurin experiments may be underestimated. None of the inhibitors alone or in combination with 10 μM 17β-E2 had prominent effects on V_{50} (ΔV_{50} was within ±7 mV; table S3). Together, these data suggest that the 17β-E2–induced reduction in G_{max} of Kv7.1/KCNE1 is dependent on conventional PKC subtypes (α, β, and γ). However, 17β-E2–induced inhibition of Kv7.1/KCNE1 could not be mimicked by simple activation of PKC using phorbol 12-myristate 13-acetate (PMA), which is a commercially available PKC activator. In contrast to the reduction in G_{max} induced by 17β-E2, acute application of 1 nM PMA increased G_{max} of Kv7.1/KCNE1 by +15 ± 6% (P < 0.05 with one-sample t test; fig. S3), an effect that was abolished by the PKC inhibitor chelerythrine (fig. S3).

17β-E2–mediated inhibition of Kv7.1/KCNE1 is dependent on S68 but not dynamin

To test whether the 17β-E2 effect on Kv7.1/KCNE1 is dependent on similar PKC-mediated pathways, as proposed for Kv7.1/KCNE3, we assessed the impact of preventing dynamin-dependent internalization or phosphorylation of the homologous predicted PKC target in KCNE1 (S68, homologous to S82 in KCNE3) (*29*), respectively. In contrast to the 17β-E2 effect on Kv7.1/KCNE3 (*25*), the dynamin inhibitor dynasore did not impair the ability of 17β-E2 to reduce G_{max} of Kv7.1/KCNE1. In the presence of dynasore, 10 μM 17β-E2 reduced G_{max} of Kv7.1/KCNE1 by −74 ± 6%, which was similar to the 17β-E2 effect in the absence of dynasore (Fig. 4, A and D, and table S3). In contrast, the serine-to-alanine mutation at position 68, which is anticipated to prevent phosphorylation at position 68, abolished 17β-E2–mediated inhibition of Kv7.1/KCNE1 (Fig. 4, B and D). ΔG_{max} for 10 μM 17β-E2 on Kv7.1/KCNE1_S68A was −14 ± 4% ($P > 0.05$ with one-sample t test; Fig. 4, B to D). As a control, we found that a serine-to-alanine mutation of S102, a predicted PKC target outside the region of KCNE1 residues 67 to 77 identified as important for the 17β-E2, did not alter the 17β-E2 effect. Ten micromolar 17β-E2 reduced G_{max} of Kv7.1/KCNE1_S102A to a similar extent as for wild-type (WT) Kv7.1/KCNE1 (ΔG_{max} was −57 ± 6%; Fig. 4D). Notably, a serine–to–aspartic acid mutation at position 68, which is anticipated to mimic the phosphorylated form of serine at position 68, did not abolish 17β-E2–mediated inhibition of Kv7.1/KCNE1 (Fig. 4, C and D). ΔG_{max} for 10 μM 17β-E2 on the phosphomimetic Kv7.1/KCNE1_S68D mutant was −68 ± 4% ($n = 5$), which was similar to the 17β-E2 effect on WT Kv7.1/KCNE1 (Fig. 4, C and D). Moreover, the phosphomimetic S68D mutation removed the PKC dependence of the 17β-E2 effect, as the PKC inhibitor chelerythrine did not abolish the G_{max} effect of 10 μM 17β-E2 on Kv7.1/KCNE1_S68D (Fig. 4D). Together, these data suggest that the 17β-E2 effect on Kv7.1/KCNE1 is dependent on S68, but not on dynamin. Furthermore, the chelerythrine and mutagenesis data for position 68 suggest that either PKC (with S68 as predicted phosphorylation target) or a phosphomimetic side chain at position 68 is required for 17β-E2 effects.

LQTS-associated mutations in KCNE1 alter the 17β-E2 effect

In addition to the predicted PKC target S68, the region of residues 67 to 77 in KCNE1 harbors several residues for which LQTS-associated mutations or polymorphisms have been described. These mutations include R67C, S68T, K69R, K70N, H73Y, S74L, and D76N (*2*, *14*, *30*–*32*). Both autosomal heterozygous and autosomal homozygous forms of these mutations have been described, with autosomal dominant inheritance being by far the most prevalent form. To determine whether any of these LQTS-associated mutations affected the 17β-E2 effect, we tested the ability of 3 and 10 μM 17β-E2 to reduce G_{max} of each mutant. The mutants Kv7.1/KCNE1_K69R, Kv7.1/KCNE1_S74L, and Kv7.1/KCNE1_D76N showed a response to 17β-E2 comparable to that of WT Kv7.1/KCNE1 with pronounced reduction in G_{max} (Fig. 5, A and B, and table S4). In contrast, mutants Kv7.1/KCNE1_S68T and Kv7.1/KCNE1_K70N showed impaired response to 17β-E2 with a reduction in G_{max} less than half of that of WT Kv7.1/KCNE1 (Fig. 5, A and C, and table S4). Mutants Kv7.1/KCNE1_R67C and Kv7.1/KCNE1_H73Y were not inhibited by 17β-E2 [Fig. 5, A and D ($P > 0.05$ for ΔG_{max} with one-sample t test), and table S4]. These coinjection experiments with Kv7.1 and LQTS-mutant forms of KCNE1 would represent the most extreme effect that a specific KCNE1 mutation may have on its susceptibility to 17β-E2 (i.e., mimicking a homozygous setting in our coinjection experiments). To mimic a heterozygous setting, we repeated these experiments for the four LQTS mutants that showed a deviating 17β-E2 response to that of WT, this time coinjecting WT Kv7.1 with 50% mutant KCNE1 and 50% WT KCNE1. These experiments show that, in the heterozygous setting, mutant Kv7.1/KCNE1_S68T displayed a WT-like response to 17β-E2 (fig. S4), whereas mutants Kv7.1/KCNE1_R67C, Kv7.1/KCNE1_K70N, and Kv7.1/KCNE1_H73Y showed an 17β-E2 response that was intermediate to that of WT Kv7.1/KCNE1 and the homozygous setting for each mutant (fig. S4). Together, these experiments show that Kv7.1/KCNE1 channels harboring LQTS-associated mutations display a range of responses to 17β-E2, from a WT-like response to either impaired or abolished response.

LQTS-associated mutations and 17β-E2 have a combined burden on Kv7.1/KCNE1

In line with previous reports for several of the LQTS-associated mutants, all mutants showed loss of function phenotype with a V_{50} that was shifted more than 20 mV toward more positive voltages compared to that of WT Kv7.1/KCNE1 under control conditions (fig. S5 and table S5). Moreover, all mutants except Kv7.1/KCNE1_K69R generated smaller currents at +40 mV (a voltage relevant for the action potential plateau phase) compared to WT [denoted by "0 μM," $P < 0.05$ using one-way analysis of variance (ANOVA) with Dunnett's multiple comparisons test; Fig. 6A]. Kv7.1/KCNE1_S68T showed the most impaired ability to generate current (<3% of WT current amplitude), and Kv7.1/KCNE1_K69R showed the most preserved ability to generate current (about 68% of WT current amplitude).

To determine the combined burden of a mutation and 17β-E2, we multiplied this relative current amplitude of each mutant with the change in current amplitude at +40 mV for each mutant induced by 17β-E2 (i.e., 0 μM in Fig. 6A multiplied with data in fig. S6). This gave us the relative remaining current of each mutant under the influence of 17β-E2 compared to WT under control conditions (i.e., no 17β-E2). The pattern of how the steady-state current at +40 mV was affected by 17β-E2 followed the pattern of effects at G_{max}, with Kv7.1/KCNE1_K69R, Kv7.1/KCNE1_S74L, and Kv7.1/KCNE1_D76N responding with the largest current reduction induced by 17β-E2 in a concentration-dependent manner and Kv7.1/KCNE1_K70N responding with a less pronounced current reduction (Fig. 6A). In contrast, the current amplitude of Kv7.1/KCNE1_R67C and Kv7.1/KCNE1_H73Y did not show further reduction induced by 17β-E2 (Fig. 6A). The reduction in steady-state current of Kv7.1/KCNE1_S68T induced by 17β-E2 could not be reliably determined, as the currents at +40 mV generated by the Kv7.1/KCNE1_S68T mutant were too small. Together, these data suggest that whereas the function of some mutants is not further impaired by 17β-E2 (such as Kv7.1/KCNE1_R67C and Kv7.1/KCNE1_H73Y), the combined burden of the mutation and 17β-E2 results in less than 10% remaining currents of mutants such as Kv7.1/KCNE1_S74L and Kv7.1/KCNE1_D76N compared to WT Kv7.1/KCNE1 under control conditions.

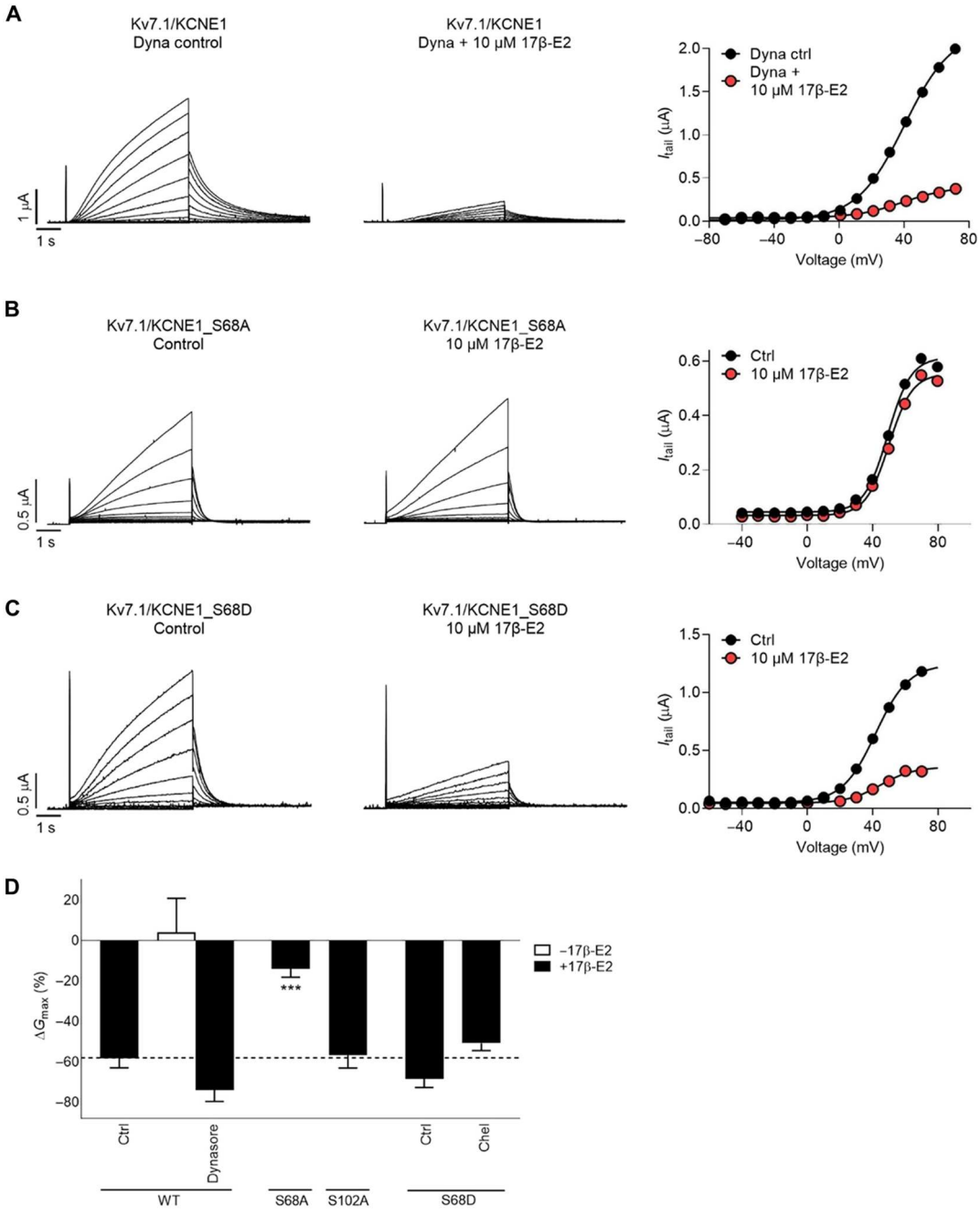

Fig. 4. 17β-E2 inhibition of Kv7.1/KCNE1 is dependent on KCNE1/S68A but not dynamin. (**A**) Representative current family with corresponding *G*(*V*) curve of dynasore-treated Kv7.1/KCNE1 in the absence (left) and presence (middle) of 10 μM 17β-E2. Curves in the *G*(*V*) plot (right) represent Boltzmann fits. For this specific cell, $V_{50,ctrl}$ = +40 mV, $I_{tailmax,ctrl}$ = 2.2 μA, $V_{50,17β\text{-}E2}$ = +39 mV, and $I_{tailmax,17β\text{-}E2}$ = 0.4 μA. (**B**) Representative current family with corresponding *G*(*V*) curve of Kv7.1/KCNE1_S68A in the absence (left) and presence (middle) of 10 μM 17β-E2. Curves in the *G*(*V*) plot (right) represent Boltzmann fits. For this specific cell, $V_{50,ctrl}$ = +49 mV, $I_{tailmax,ctrl}$ = 0.6 μA, $V_{50,17β\text{-}E2}$ = +50 mV, and $I_{tailmax,17β\text{-}E2}$ = 0.6 μA. (**C**) Same as in (B) but for Kv7.1/KCNE1_S68D. For this specific cell, $V_{50,ctrl}$ = +42 mV, $I_{tailmax,ctrl}$ = 1.2 μA, $V_{50,17β\text{-}E2}$ = +45 mV, and $I_{tailmax,17β\text{-}E2}$ = 0.4 μA. (**D**) Summary of the effect of 10 μM 17β-E2 on Kv7.1/KCNE1 channels with indicated inhibitor or KCNE1 mutations. Data are shown as means ± SEM. *n* = 3 to 18. Statistics indicate one-way ANOVA followed by Dunnett's multiple comparisons test to determine whether the 17β-E2 effect deviates from the effect on WT (included as bar marked "Ctrl"). ***$P < 0.001$. $P > 0.05$ (n.s.) for all other data (see also table S3). Open bar ("-17β-E2") denotes Kv7.1/KCNE1 exposed to the indicated inhibitor in the absence of 17β-E2 (see Materials and Methods for details). The black dashed line indicates the effect of 10 μM 17β-E2 on WT Kv7.1/KCNE1.

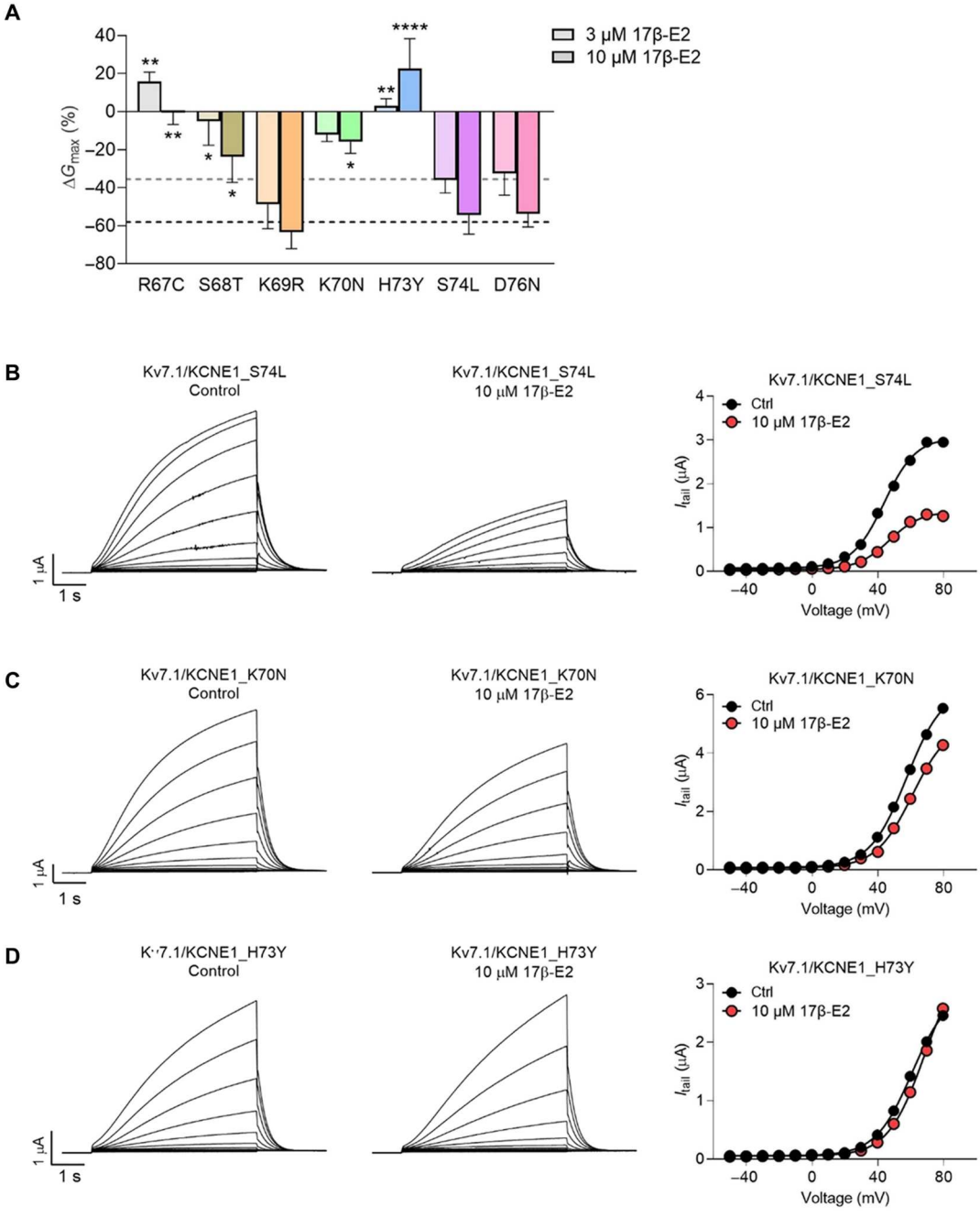

Fig. 5. LQTS-associated mutations in KCNE1 alter the 17β-E2 effect. (**A**) Summary of the effect of 3 and 10 μM 17β-E2 on Kv7.1/KCNE1 channels with indicated LQTS-associated mutations in KCNE1. Data are shown as means ± SEM. n = 3 to 10 (defined in table S4). Statistics indicate one-way ANOVA followed by Dunnett's multiple comparisons test to determine whether the 17β-E2 effect on mutated channels deviates from the effect on WT. *P < 0.05, **P < 0.01, and ****P < 0.0001. P > 0.05 (n.s.) for all other data (see table S4). Gray and black dashed lines indicate the effect of 3 and 10 μM 17β-E2, respectively, on WT Kv7.1/KCNE1. (**B**) Representative current family with corresponding $G(V)$ curve of Kv7.1/KCNE1_S74L in the absence (left) and presence (middle) of 10 μM 17β-E2. Curves in the $G(V)$ plot (right) represent Boltzmann fits. For this specific cell, $V_{50,ctrl}$ = +44 mV, $I_{tailmax,ctrl}$ = 3.1 μA, $V_{50,17β\text{-}E2}$ = +47 mV, and $I_{tailmax,17β\text{-}E2}$ = 1.4 μA. (**C**) Same as in (B) but for Kv7.1/KCNE1_K70N. For this specific cell, $V_{50,ctrl}$ = +57 mV, $I_{tailmax,ctrl}$ = 6.2 μA, $V_{50,17β\text{-}E2}$ = +61 mV, and $I_{tailmax,17β\text{-}E2}$ = 5.1 μA. (**D**) Same as in (B) but for Kv7.1/KCNE1_H73Y. For this specific cell, $V_{50,ctrl}$ = +61 mV, $I_{tailmax,ctrl}$ = 2.9 μA, $V_{50,17β\text{-}E2}$ = +68 mV, and $I_{tailmax,17β\text{-}E2}$ = 3.5 μA.

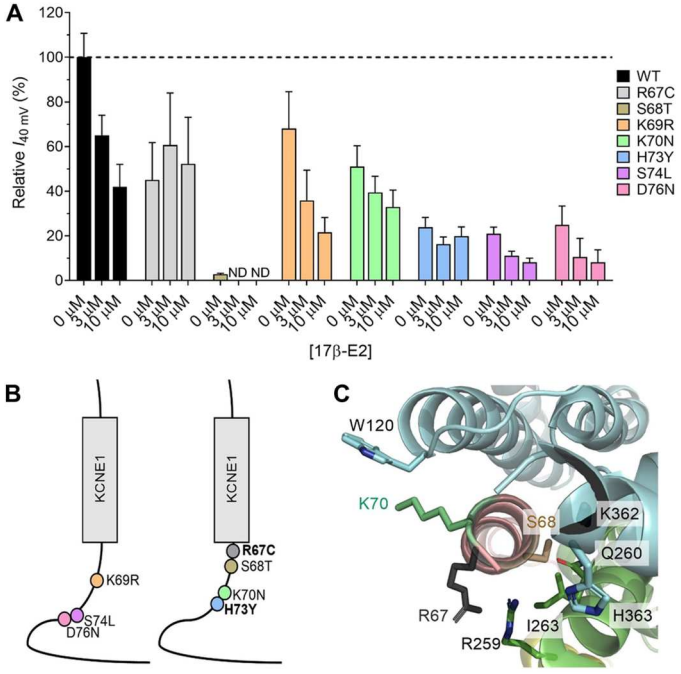

Fig. 6. Determining the combined burden of LQTS-associated mutation and 17β-E2 effect. (**A**) The relative steady-state current amplitude at +40 mV of indicated Kv7.1/KCNE1 LQTS-associated mutants under control conditions (0 μM) and in the presence of 3 and 10 μM 17β-E2 ("3 μM" and "10 μM," respectively), normalized to the current amplitude of WT Kv7.1/KCNE1 under control conditions. The combined burden of a mutation and 17β-E2 was determined by multiplying the control amplitude for each mutant [0 μM in (A)] with the mean 17β-E2–induced decrease in steady-state current amplitude at +40 mV (reported in fig. S8). See Materials and Methods for details. Data are shown as means ± SEM. n = 3 to 10. ND denotes not determined because of unquantifiable current amplitudes of the S68T mutant at +40 mV. (**B**) Schematic illustration of KCNE1 highlighting LQTS-associated mutations in KCNE1 with preserved WT-like response to 17β-E2 (left) and mutations with reduced (S68T and K70N) or abolished (R67C and H73Y) response to 17β-E2. (**C**) Bottom view of Kv7.1/KCNE1 highlighting proposed interactions between the C terminus of KCNE1 and the lower part S1 (e.g., W120), S5 (e.g., R259, Q260, and I263), and S6 (e.g., K362 and H363) of Kv7.1. Figure inspired by (*46*) and made using their model of Kv7.1/KCNE1 in the activated open state (PDBDEV: 00000042). Note that H73 is in an unresolved region and not included in the model.

17β-E2, at physiological concentrations, reduces I_{Ks} in rabbit cardiomyocytes

To validate the 17β-E2 effect on I_{Ks} observed in *Xenopus* oocytes also in mammalian cells, we performed additional experiments in isolated rabbit ventricular cardiomyocytes. We chose rabbits, as pronounced similarities in terms of cardiac electrophysiology exist between rabbits and humans; in particular, the main repolarizing currents, the rapid and slow delayed rectifier K^+ currents (I_{Kr} and I_{Ks}), are present in both species (*33*). Here, we aimed to test whether a 17β-E2–mediated I_{Ks} inhibition was also detectable in a more physiological concentration (such as 3 nM 17β-E2 that is reached during pregnancy; reference ranges from the American College of Physicians and the Mayo Clinic). In the presence of the two concentrations tested, 3 μM and 3 nM, 17β-E2 reduced I_{Ks} significantly (Fig. 7, A to C), confirming the validity of the 17β-E2 effects on Kv7.1/KCNE1 observed in the *Xenopus* oocyte experiments. The fact that 3 nM 17β-E2 induced a prominent reduction in I_{Ks}, with no further reduction induced by the higher 3 μM 17β-E2, suggests that saturating 17β-E2 effects on I_{Ks} most likely already occur at low (or sub) nanomolar concentrations in rabbit cardiomyocytes.

The 17β-E2 effects on I_{Ks} observed in rabbit cardiomyocytes occurred at considerably lower concentrations than those observed on Kv7.1/KCNE1 in the *Xenopus* oocytes. Although several aspects differ between these two experimental models, we were interested in the putative role of the use of dimethyl sulfoxide (DMSO) as the 17β-E2 stock solvent in the rabbit cardiomyocyte experiments [in contrast to ethanol (EtOH) used in *Xenopus* oocyte experiments]. A reason for further investigating this aspect was a recent study (*34*) on another lipophilic compound, cannabidiol, which elegantly shows limited cannabidiol accessibility and binding of cannabidiol to plastic containers and tubing, greatly reducing the pharmacologically available concentration in the solution and, hence, the apparent effects of cannabidiol at submicromolar concentrations. Because studies have shown impaired solubility profile of 17β-E2 from EtOH stocks compared to DMSO stocks (*35*), we reasoned that 17β-E2 may behave similar as cannabidiol and that the use of DMSO as the solvent may prevent 17β-E2 binding to the plastic material and improve overall 17β-E2 accessibility in *Xenopus* oocyte experiments. Hence, we performed key control experiments of 17β-E2 effects on Kv7.1/KCNE1 in the *Xenopus* oocytes, this time using DMSO as the 17β-E2 stock solvent. Under these experimental conditions, 17β-E2 induced pronounced reduction of current amplitude at +40 mV and G_{max} already at nanomolar concentrations (Fig. 7D). The expected maximal 17β-E2 effect on current amplitude at +40 mV was −77% with an median effective concentration (EC_{50}) of 185 nM (Fig. 7D). The corresponding numbers for G_{max} were −79% and 241 nM. However, the choice of stock solvent affected only the 17β-E2 concentrations required to induce effects but not the pattern of effects. Like in experiments using EtOH as the stock solvent, Kv7.1 alone was unresponsive to 17β-E2 with DMSO as the stock solvent (Fig. 7E). Moreover, 17β-E2 with DMSO as the stock solvent affected the S74L mutant in a WT-like manner, whereas the H73Y mutant was unaffected (Fig. 7F), in line with experiments shown in Figs. 5 and 6.

Combined, these experiments show that physiologically relevant concentrations of 17β-E2 can inhibit I_{Ks} and that the range of concentrations required to induce effects largely depends on technical aspects of the experiments (such as the choice of stock solvent to increase the overall accessibility of 17β-E2 and prevent binding to plastic material).

DISCUSSION

In this study, we show that 17β-E2 inhibits human Kv7.1/KCNE1 expressed in *Xenopus* oocytes, whereas the other vital steroid sex hormones estrone, estriol, progesterone, and testosterone are without effect. We find that the KCNE1 subunit is required for this inhibitory 17β-E2 effect and that the effect is tuned by the stoichiometry of Kv7.1 to KCNE1 with reduced 17β-E2 effects upon KCNE1 reduction. Within KCNE1, we identify a stretch of the C terminus critical for the 17β-E2 effect. This KCNE1 region harbors several loss-of-function LQTS-associated mutations, which we find display mutation-specific responses to 17β-E2

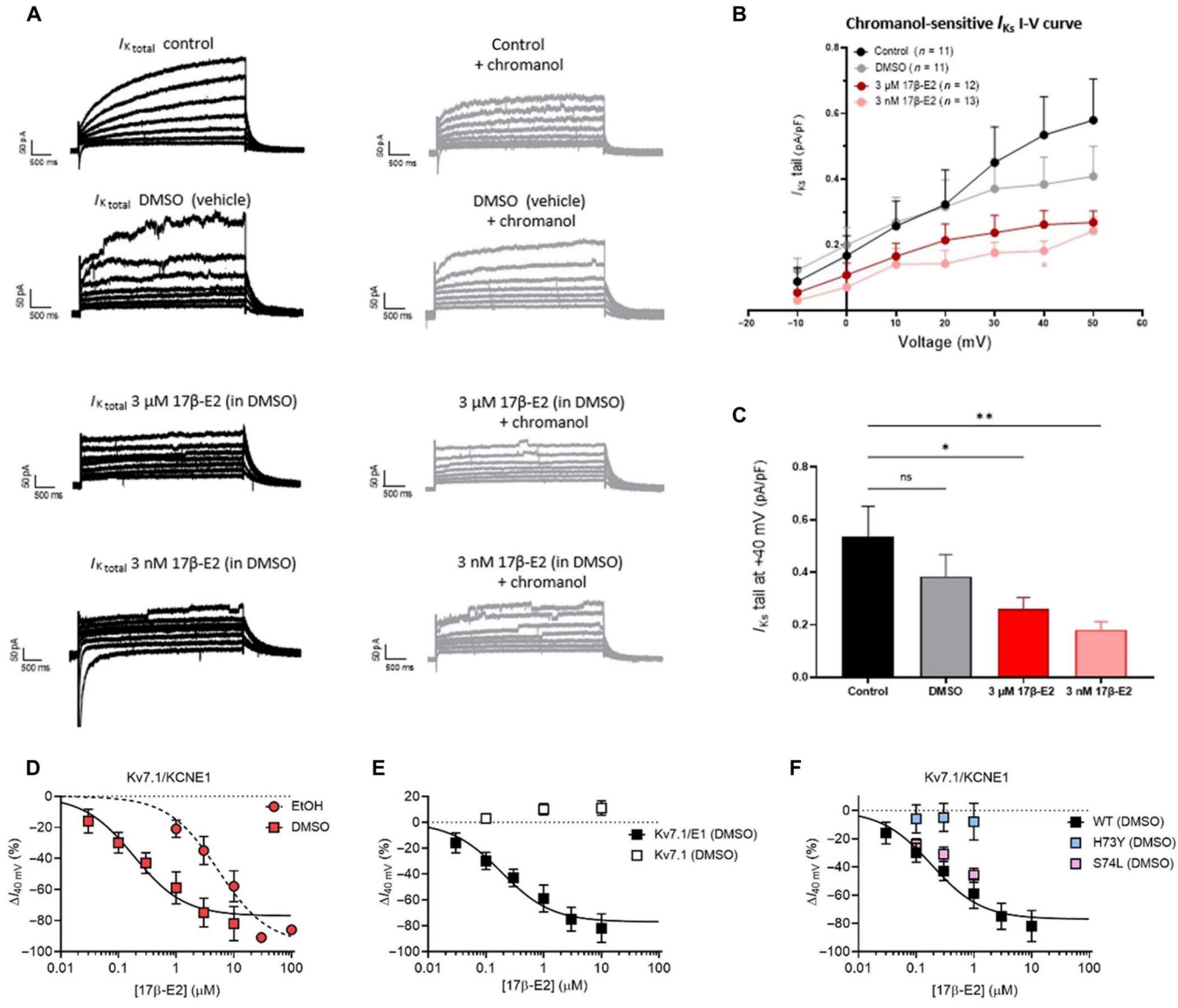

Fig. 7. 17β-E2 effect on tail current of I_{Ks} in ventricular cardiomyocytes isolated from female rabbits. (**A**) Representative current traces in the absence (black) or presence (gray) of 30 µM chromanol 293B in a control cell (C_m = 128 pF) and in a cell incubated with 0.06% (v/v) DMSO (C_m = 132 pF) or 3 µM 17β-E2 (C_m = 248 pF) or 3 nM 17β-E2 (C_m = 147 pF). (**B**) I_{Ks} tail current-voltage (*I-V*) relationships, using the voltage protocol indicated in Materials and Methods. I_{Ks} was obtained as chromanol 293B (30 µM)–sensitive current. Values are shown in the figure as means ± SEM. Statistical analysis was performed using two-way ANOVA followed by Bonferroni post hoc analysis. (**C**) Effect of 17β-E2 on I_{Ks} tail at +40 mV. Data are shown as means ± SEM. Statistical analysis was performed using one-way ANOVA followed by Bonferroni post hoc analysis. (**D** to **F**) Summary of the effect of 17β-E2 with DMSO as stock solvent on indicated constructs expressed in *Xenopus* oocytes. (**D**) Concentration dependence of the 17β-E2 effect on current amplitude at +40 mV of Kv7.1/KCNE1 upon dissolving 17β-E2 in DMSO. The curve represents concentration-response fit. Best fit, maximum $\Delta I_{40\,mV}$ = −77% and EC_{50} = 185 nM. Data are shown as means ± SEM. n = 3 to 8. The corresponding data for 17β-E2 dissolved in EtOH (from Fig. 1G) is included for comparison. (**E**) Lack of effect of 17β-E2 dissolved in DMSO on Kv7.1 alone, in line with experiments using 17β-E2 dissolved in EtOH (shown in fig. S1A). Data are shown as means ± SEM. n = 5. (**F**) Preserved WT-like response of the S74L mutation and abolished response of the H73Y mutation to 17β-E2 dissolved in DMSO, in line with experiments using 17β-E2 dissolved in EtOH (shown in Figs. 5 and 6). Data are shown as means ± SEM. n = 3 to 5.

ranging from a WT-like response (Fig. 6B, left) to reduced or abolished response (Fig. 6B, right). Moreover, we could validate these findings in mammalian cardiomyocytes, in which similar I_{Ks}-inhibitory 17β-E2 effects were found.

The rapid and concentration-dependent inhibition of Kv7.1/KCNE1 described here is in line with previous studies of 17β-E2 effects on Kv7.1/KCNE1 in *Xenopus* oocytes, Chinese hamster ovary cells (*36*, *37*), and native I_{Ks} in animal models (*16*, *38*, *39*). However, the underlying mechanisms for 17β-E2–induced Kv7.1/KCNE1 inhibition have been poorly understood. In analogy with 17β-E2–mediated inhibition of another channel complex composed of Kv7.1 and another β-subunit from the KCNE family, Kv7.1/KCNE3, which plays a physiological role in the sexual dimorphism and estrous cycle dependence of the antisecretory actions of

estrogen in the intestine (*27*), we found the 17β-E2 effect to be dependent on PKC and a predicted PKC target in the KCNE C terminus (S68 in KCNE1). However, our data suggest that although there are similarities in the 17β-E2 effect on Kv7.1/KCNE1 and Kv7.1/KCNE3, channel inhibition of the two Kv7.1/KCNE channel complexes are not mediated through similar mechanisms. Whereas the 17β-E2 effect on Kv7.1/KCNE3 is attributed to dynamin-dependent channel internalization (upon phosphorylation of dynamin) and dissociation of KCNE3 from Kv7.1 (upon phosphorylation of S82 in KCNE3) (*25*–*27*), we do not find support of similar underlying mechanisms for Kv7.1/KCNE1. In our hands, the 17β-E2 effect on Kv7.1/KCNE1 was not impaired upon inhibition of dynamin-dependent internalization, and we saw no sign of KCNE1 dissociation from Kv7.1 (which would have been observed as Kv7.1-like currents upon 17β-E2 application). Moreover, direct activation of PKC using PMA did not recapitulate the 17β-E2 effect on Kv7.1/KCNE1. Thus, the assessment of 17β-E2 effects on Kv7.1/KCNE1 in the present study, which, in the initial experiments, largely follows previous studies of Kv7.1/KCNE3, allows for identification of similarities and important differences in 17β-E2–mediated channel inhibition of the two Kv7.1/KCNE channel complexes.

In addition to triggering signaling pathways, 17β-E2 has been shown to directly bind to ion channels to modulate channel activity (*40*–*43*). One possibility is that the 17β-E2 effect on Kv7.1/KCNE1 also involves direct 17β-E2 binding to the channel. The KCNE1 region encompassing residues 67 to 73, identified in this study to be important for 17β-E2 effects, has been shown to interact with several regions on Kv7.1 including the lower end of S6 of Kv7.1 (Fig. 6C) (*44*, *45*), interactions that are proposed to contribute to stabilizing the open gate of Kv7.1/KCNE1 (*46*). Either indirect conformational rearrangements induced by 17β-E2 or direct 17β-E2 binding to this region could potentially inhibit Kv7.1/KCNE1 by disrupting these interactions. In this context, we find the PKC dependence of the 17β-E2 effect and the putative role of the predicted PKC target S68 intriguing. That the 17β-E2 effect is abolished in the S68A mutant (which is unable to be phosphorylated), retained in the S68D mutant (which is mimicking the phosphorylated serine side chain), and no longer PKC dependent in the S68D mutant is compatible with a model, in which a phosphorylated/phosphomimetic side chain at position S68 is required to allow for 17β-E2 effects. Altered pharmacology upon channel phosphorylation was recently described for Nav1.5, in which phosphorylation of tyrosine Y1495 is proposed to impair quinidine inhibition of the channel by inducing a conformational change unfavorable for quinidine binding (*47*). However, given the multiple and complex mechanisms by which 17β-E2 affects ion channels, including altered exocytosis, internalization, and/or gating (*19*, *25*, *40*), the relationship between direct and indirect mechanisms contributing to 17β-E2 inhibition of Kv7.1/KCNE1 needs to be investigated in future work. Such work could favorably include studies of a putative role of phosphatidylinositol 4,5-bisphosphate (PIP_2) and calmodulin, as 17β-E2 signaling may influence PIP_2 levels (*19*) and the interface between the C terminus of KCNE1 and Kv7.1 highlighted in Fig. 6C is important for both PIP_2 and calmodulin effects (*46*, *48*, *49*).

Although sex differences in cardiac repolarization and arrhythmic risk have been experimentally linked to sex differences in repolarizing potassium current densities, namely, I_{Kr}, I_{Ks}, I_{to}, and I_{K1}, and contrasting effects of male and female sex hormones on these currents [reviewed in (*8*)], thus far, only limited data are available on direct effects of 17β-E2 on Kv7.1/KCNE1 channels and the corresponding I_{Ks} currents. Indirect evidence for an I_{Ks}-reducing effect of 17β-E2 stems from the observation of down-regulation of KCNE1 mRNA levels by 17β-E2 (*16*). This study now adds evidence for additional direct inhibiting effects of 17β-E2 on Kv7.1/KCNE1 that are mediated by the C terminus of the channels′ auxiliary subunit KCNE1, which could be one contributing factor to the longer QT duration and higher arrhythmic risk in postpubertal women than in men. The inhibiting effect of 17β-E2 on Kv7.1/KCNE1 may be of particular importance in cases with already impaired repolarization capacity, such as for carriers of loss-of-function Kv7.1/KCNE1 mutations. In our hands, this is exemplified by the LQTS-associated mutations K69R, S74L, and D76N, which showed an even greater loss of function upon 17β-E2 exposure. In contrast, the reduced or abolished Kv7.1/KCNE1 response of LQTS-associated mutations R67C, S68T, K70N, and H73Y to 17β-E2 suggest that 17β-E2 may not be an additional QT-prolonging risk factor (i.e., not further aggravating Kv7.1/KCNE1 loss of function) in such carriers. Note, however, that as 17β-E2 also acts on other channels, there might still be some sex differences that are due to other 17β-E2 effects. Whether our observations of less or more pronounced susceptibility to 17β-E2–induced I_{Ks} reduction in different KCNE1 variants translate clinically into more or less pronounced sex differences in these LQT subtypes remains to be investigated. While pronounced sex differences in QT duration and arrhythmic risk are known in LQTS patients with a longer QT duration and increased risk in women (*12*) and estrous cycle–dependent changes in QT intervals (*50*), these data mainly stem from patients with the most frequent LQTS genotypes associated with mutations in *KCNQ1* (LQT1) and *KCNH2* (LQT2). It is less clear in the much rarer forms caused by mutations in *KCNE1* (LQT5) due to the paucity of clinical data of this rare form of LQTS. For our here investigated LQT5 mutations, too little clinical data on affected patients are available to conclusively determine whether the specific mutations cause sex differences in QT duration and arrhythmias or even estrous cycle–dependent changes in arrhythmic risk. However, for the common KCNE1 polymorphism pD85N, a sex-specific modulatory effect of the susceptibility to drug-induced LQTS has already been described with 17β-E2–mediated exaggeration of dofetilide-induced APD prolongation and increase in proarrhythmic early afterdepolarizations in induced pluripotent stem cell-derived cardiomyocytes (iPSC-CMs) (*51*), pointing toward a normal WT-like inhibitory 17β-E2 effect on Kv7.1/KCNE1_D85N and strongly supporting a role of KCNE1 variants in mediating (parts of) the observed sex differences in LQTS.

An important technical discovery made in this study was the great impact of the choice of 17β-E2 solvent for achieving effects at submicromolar concentrations. With the use of DMSO as solvent, we find inhibiting 17β-E2 effects on both I_{Ks} in rabbit cardiomyocytes and Kv7.1/KCNE1 expressed in *Xenopus* oocytes at concentrations in line with reported plasma concentrations, which range from low nanomolar concentrations to 0.1 μM (reference ranges from the American College of Physicians and the Mayo Clinic). Similarly, some previous studies have shown that physiological, low nanomolar concentrations of 17β-E2 are enough to inhibit the cardiac hERG channel underlying I_{Kr} and prolong action potential duration in cardiomyocytes (*52*), whereas many studies report that concentrations in the micromolar range are needed to induce

comparable hERG inhibition and action potential prolongation in different cellular systems (*37*, *39*, *53*, *54*). The reason why some experimental settings allow us to investigate 17β-E2 effects at nanomolar concentrations and others require micromolar concentrations remains, in most cases, unknown, but may, to some extent, reflect the use of different cell types and experimental temperatures (*53*). Our study suggests that one contributing factor could be the choice of 17β-E2 solvent, where DMSO appears to provide better experimental conditions for assessing the effect of low 17β-E2 concentrations.

Limitations of our study include the focused studies of 17β-E2 effects on Kv7.1/KCNE1, given that 17β-E2 effects on ion currents in vivo are multiple and complex. Thus, while our experimental system offers strength for investigating the mechanism of 17β-E2 effects on Kv7.1/KCNE1 due to robust expression of ion channels and minimal endogenous interference, more intricate experimental systems are required to capture the full complexity of 17β-E2 effects. Moreover, our experimental setting does not consider the different fractions of 17β-E2 in vivo, which includes unbound 17β-E2 and 17β-E2 bound to, for instance, albumin and sex hormone binding globulin. Hence, in addition to the above-mentioned technical challenges related to available 17β-E2 concentrations, the role of 17β-E2 carrier proteins would need to be studied in a more physiological setting, with the aim of recapitulating the dynamics of 17β-E2 and other ligands binding and dissociating from such carrier proteins. Limitations also include the challenge of subtype selectivity of PKC inhibitors. Many PKC subtypes are closely related, and even inhibitors reported to be relatively selective for one subtype may target additional PKC subtypes (*55*). Therefore, the specificity of PKC inhibitors should be interpreted with caution.

Together, our study expands the mechanistic understanding of 17β-E2–mediated inhibition of Kv7.1/KCNE1 and identifies LQTS-associated mutations in the C terminus of KCNE1 that alter the 17β-E2 effect. The important role of KCNE1 in terms of how Kv7.1/KCNE1 responds to pharmacological compounds and the action of accessory molecules such as calmodulin and adenosine triphosphate (ATP) and phosphorylation is well established (*56*–*58*). Our findings of the importance of the KCNE1 C terminus for 17β-E2 effects add to this complexity. Moreover, the finding that KCNE1 is required for the inhibitory 17β-E2 effect together with the previous finding of an 17β-E2–induced down-regulation of KCNE1 mRNA by Drici and co-workers (*16*) suggests that 17β-E2 may regulate/limit its own Kv7.1/KCNE1-inhibitory effect by regulating KCNE1 expression. A fascinating, but challenging, aspect of LQTS is that several concomitant QT-prolonging factors seem, in many cases, to be required to induce the LQTS phenotype (*7*). Our study suggests that the combined burden of LQTS mutations and 17β-E2 influence may constitute an important example.

MATERIALS AND METHODS

Chemicals

All chemicals were purchased from Sigma-Aldrich (Stockholm, Sweden) unless stated otherwise. G15 was from MedChemtronica AB (Sollentuna, Sweden). Stock solutions of hormones were prepared in 99.5% EtOH to a concentration of 10 mM (estriol) or 25 mM (all other hormones). In experiments shown in Fig. 7, the stock solution of 17β-E2 was prepared in DMSO to a concentration of 10 mM. Stock solution of PMA was prepared in 99.5% EtOH to a concentration of 20 μM. Stock solutions of antagonists were prepared according to the manufacturers' instructions with fulvestrant (25 mM), G15 (10 mM), H89 (4 mM), chelerythrine (10 mM), HBBDE (25 mM), and dynasore (50 mM) prepared in 99.5% EtOH and ruboxistaurin (1 mM), rottlerin (30 mM), and PKCε inhibitor peptide (12 mM) prepared in DMSO. Stock solutions were stored at −20°C and diluted to the final test solution concentration on the day of the experiment.

Molecular biology and oocyte preparation

Human Kv7.1 (GenBank accession no. NM_000218) and KCNE1 (NM_000219) were used in this study. Mutations were introduced through site-directed mutagenesis (QuikChange II XL, with 10XL-Gold cells; Agilent Technologies, Kista, Sweden) and confirmed by sequencing at the Linköping University Core Facility. KCNE1_Δ2-38, KCNE1_Δ67, and concatenated constructs have been described before (*59*, *60*). KCNE1_Δ78, KCNE1_Δ80, and KCNE1_Δ102 were constructed by introducing a stop codon at indicated residue. Complementary RNA (cRNA) for injection was prepared from DNA using a mMESSAGE mMACHINE T7 transcription kit (Invitrogen, Stockholm, Sweden), and cRNA concentrations were determined by means of spectrophotometry (NanoDrop 2000c, Thermo Scientific, Stockholm, Sweden). Isolated oocytes from *X. laevis* frogs were acquired either through surgical removal followed by enzymatic digestion at Linköping University or purchased from Ecocyte Bioscience (Dortmund, Germany). The use of animals (female *X. laevis* frogs; age, 10 months to 5 years; no genetic modification; Nasco, WI, USA), including the performed surgery, followed Institutional Animal Care and Use Committee guidelines and was reviewed and approved by the regional board of ethics in Linköping, Sweden (case no. 1941). cRNA (50 nl) was injected into oocytes at developmental stages V to VI (Drummond Scientific, PA, USA). For coinjection of Kv7.1 and KCNE1, each oocyte received 25 ng of Kv7.1 RNA and 8 ng of KCNE1 RNA. For coinjection of Kv7.1 and mutant KCNE1 in conditions mimicking a heterozygous setting, each oocyte received 25 ng of Kv7.1 RNA, 4 ng of WT KCNE1 RNA, and 4 ng of mutant KCNE1 RNA. For injection of Kv7.1 alone or concatenated channels, each oocyte received 50 ng of RNA. Concatenated KCNE1-Kv7.1 channels, promoting either a 4:4 or 2:4 stoichiometry of KCNE1 to Kv7.1, were primarily used to assess the 17β-E2 effect on channels with different numbers of KCNE1 subunits (which is less controlled in our regular coinjection experiments, although we anticipate mainly a 4:4 stoichiometry due to the excess of KCNE1 RNA). Moreover, because the KCNE1 to Kv7.1 stoichiometry of the native cardiac I_{Ks} channel complex is debated, we were interested in studying whether the number of KCNE1 subunits in the complex made a difference. Injected oocytes were incubated at 8° or 16°C for 2 to 8 days before electrophysiological experiments in Modified Barth's Solution consisting of 88 mM NaCl, 1 mM KCl, 2.4 mM $NaHCO_3$, 0.33 mM $Ca(NO_3)_2$, 0.41 mM $CaCl_2$, 0.82 mM $MgSO_4$, 15 mM Hepes, and 2.5 mM pyruvate, with pH set to 7.6 using NaOH.

Two-electrode voltage clamp experiments on *Xenopus* oocytes

Two-electrode voltage clamp recordings were performed at room temperature with an Axon AxoClamp 900A amplifier system (Molecular Devices Ltd., Wokingham, UK) or a Dagan CA-1B amplifier system (Dagan, MN, USA). Pulled microelectrodes (0.4 to 1.5

megohms; World Precision Instruments Inc., FL, USA) were filled with 3 mM KCl. Whole-cell K^+ currents were sampled using Clampex (Molecular Devices Ltd., Wokingham, UK) at 5 kHz and filtered at 500 Hz. For most experiments, the holding potential was set to −80 mV, and current families were recorded in incremental test steps of 10 mV from −80 to +70 mV, followed by a tail step to −20 mV. For Kv7.1/KCNE1, the test pulse lasted for 5 s, and for Kv7.1, the test pulse lasted for 2 s. The voltage range of test steps was adjusted for mutants with deviating voltage dependence. The sweep-to-sweep interval was 30 s. The recording control solution consisted of 88 mM NaCl, 1 mM KCl, 0.4 mM $CaCl_2$, 0.8 mM $MgCl_2$, and 15 mM Hepes, with pH set to 7.4 using NaOH. Control solution or control solution supplemented with test compounds was continuously perfused through the recording chamber (1 ml/min) using a pump (Harvard Apparatus MPII, CMA Microdialysis, Kista, Sweden, or MINIPULS 3 peristaltic pump, Gilson, WI, USA). Each test substance was applied until a stable effect on current amplitude was observed (or for a maximum of 12 min), monitored by running an application protocol stepping from a holding voltage of −80 mV to a test voltage of +20 mV every 10 s. The tubing system and recording chamber were cleaned between cells with 70% EtOH and distilled H_2O. For hERG, current families were recorded in incremental test steps of 10 mV for 2 s from −80 to +40 mV, followed by a tail step to −40 mV.

Electrophysiological analysis

GraphPad Prism 8 (GraphPad Software Inc., CA, USA) was used for data analysis. The voltage dependence of the channel opening was approximated by plotting the immediate tail currents (recorded upon stepping to the tail voltage) against the preceding test voltages. Data were fitted with a Boltzmann function to generate conductance versus voltage [$G(V)$] curves

$$G(V) = G_{min} + (G_{max} - G_{min}) / \left\{1 + \exp\left[\frac{(V_{50} - V)}{s}\right]\right\} \quad (1)$$

where G_{min} is the minimal conductance, G_{max} is the maximal conductance, V_{50} is the midpoint (i.e., the voltage required to reach half the maximal conductance in the Boltzmann fit), and s is the slope of the curve. The slope (s) was constrained to be equal for control and test compound curves in each oocyte. The relative difference between G_{max} obtained with control solution and test compound solution for each oocyte (the ΔG_{max}) was used to quantify changes in the maximum conductance evoked by test compounds. The difference between V_{50} obtained in control solution and test compound solution for each oocyte (the ΔV_{50}) was used to quantify shifts in the voltage dependence of the channel opening evoked by test compounds. For experiments where conductance did not clearly show signs of saturation in the experimental voltage range, these fits should be considered as an approximation. Table S5 summarizes the basic biophysical properties of used constructs. The 17β-E2 effect on hERG was quantified in line with previous studies (*52*) by quantifying the peak tail current amplitude measured at −40 mV after test pulses to +20 mV before and after application of 17β-E2.

To plot the concentration dependence of the 17β-E2 effect on G_{max}, the following concentration-response curve was fitted to the data

$$\Delta G_{max} = \text{maximal}\Delta G_{max} / \left[1 + \left(\frac{[IC_{50}]}{[C]}\right)^{-1}\right] \quad (2)$$

where maximalΔG_{max} is the maximal effect on G_{max}, C is the concentration of 17β-E2, and IC_{50} is the 17β-E2 concentration needed to cause 50% of the maximal effect.

To estimate the relative current generated by each LQTS-associated mutation compared to WT under control conditions (0 μM in Fig. 6), the current amplitude of mutants determined at the end of the 5 s long test pulse to +40 mV was normalized to the current amplitude of WT Kv7.1/KCNE1 expressed in the same batch of oocytes that were incubated under identical conditions. The human ventricular action potential has a systolic voltage range of about 0 to +40 mV (*61*, *62*). A potential of +40 mV was the lowest voltage for which we could reliably determine current amplitude for all mutants. To estimate the ability of 17β-E2 to further reduce current amplitude at +40 mV ("3 and 10 μM" in Fig. 6), we quantified for each mutant the mean 17β-E2–induced decrease in steady-state current amplitude at +40 mV during the 17β-E2 experiments reported in Fig. 5. The mean 17β-E2–induced decrease in steady-state current amplitude (reported in fig. S5) was then multiplied with the control amplitude for each mutant (0 μM in Fig. 6). This multiplication approach allowed us to estimate the combined burden of a mutation and 17β-E2. This approach has been previously used to estimate the combined effect of mutations and channel activators (*63*).

Experiments with receptor and kinase inhibitors or activators

To test signaling pathways involved in the 17β-E2 effect, inhibitors of classical ERs (fulvestrant), GPR30 (G15), PKAs (H89), PKCs (chelerythrine, HBBDE, ruboxistaurin, rottlerin, and PKCε inhibitor peptide), and dynamin (dynasore) were used. Oocytes were first pretreated with each inhibitor in 96-well plates with inhibitor-supplemented control recording solution at 16°C for 30 to 180 min. The concentration and incubation times of each inhibitor were selected on the basis of previous reports, which, as far as possible, included assessment in *Xenopus* oocytes (see details in table S6). Used concentrations and incubation times were as follows: 1 μM G15 for 180 min, 50 μM H89 for 180 min, 20 μM chelerythrine for 30 min, 50 μM HBBDE for 180 min, 40 nM ruboxistaurin for 90 min, 5 μM rottlerin for 60 min, 1 μM PKCε inhibitor peptide for 120 min, 80 μM dynasore for 40 min, and 10 μM fulvestrant for a minimum of 24 hours (10 μM fulvestrant showed a stable basal effect after 170 min incubation, and the 17β-E2 effect remained similar following 170 min to 72 hours of preincubation with fulvestrant). Data for a minimum of 24 hours of preincubation are included in Fig. 3 and table S3. In addition, because of the reported limited membrane permeability of PKCε inhibitor peptide on *Xenopus* oocytes (*64*), a second dataset with the PKCε inhibitor peptide was collected with 50 nl of 100 nM PKCε inhibitor peptide injected into each oocyte 15 min before 17β-E2 experiments. After pretreating the cells, the baseline current family was recorded under perfusion with control solution supplemented with inhibitor (same concentration as during pretreatment). Then, the 17β-E2 effect was recorded as in the other 17β-E2 experiments but with the control solution and 17β-E2 still supplemented with the inhibitor. Time-matched controls (open bars in Figs. 3A and 4C) of the effect

of the inhibitor in the time range used to assess 17β-E2 effects were performed in the same manner but without 17β-E2 added to the control solution. The PKC activator PMA was acutely administered with perfusion at a concentration of 1 nM for up to 20 min.

Rabbit cell isolation and whole-cell patch clamp experiments

All animal experiments were performed in compliance with European Union legislation (directive 2010/63/EU) and the Swiss Animal Welfare Ordinance after approval by the Cantonal Veterinary Office and the Animal Welfare Officer (Kanton Bern, approval number BE131-20). New Zealand White female rabbits (13 to 14 weeks old) were anesthetized with an intramuscular injection of ketamine S (12.5 mg/kg) and xylazine (3.75 mg/ml). A standard enzymatic digestion was used to isolate ventricular cardiomyocytes from five rabbits (*65*). After euthanasia with intravenous pentobarbital injection, hearts were rapidly excised, cannulated by the aorta, and mounted on a Langendorff perfusion system, where they were washed with oxygenated, body-temperature Tyrode solution. Shortly afterward, 0.1 mM EGTA-supplemented Tyrode was perfused for 5 to 7 min, followed by a 20 to 25 min step of collagenase digestion (Worthington type 1) in 80 μM Ca^{2+} Tyrode. The heart was then removed from the perfusion system and reduced into small pieces. The process was followed by sequential 5-min steps of collagenase digestion in 80 μM Ca^{2+} Tyrode buffered with 15 mM bovine serum albumin.

To elucidate the acute 17β-E2 effects on the slow component of the delayed rectifier potassium current (I_{Ks}), isolated rabbit cardiomyocytes were incubated for 2 to 5 hours with 3 nM or 3 μM 17β-E2 (dissolved in DMSO) or 0.06% (v/v) DMSO as vehicle control. Whole-cell configuration of the patch clamp technique was used to record the I_{Ks} current-voltage curve at 37°C (ThermoClamp-1, AutoMate Scientific Inc.) using an Axopatch 200B amplifier (Axon Instruments). The patch pipette solution consisted of 125 mM KCl, 5 mM NaCl, 1 mM $MgCl_2$, 5 mM K_2ATP, 10 mM Hepes, and 5 mM EGTA. The extracellular solution consisted of standard 1.8 mM Ca^{2+} Tyrode solution supplemented with 5 mM 4-aminopyridine, 10 nM nisoldipine, and 2 mM BaCl. I_{Ks} current density was identified as the chromanol 293B (30 μM)–sensitive current. To record I_{Ks}, depolarizing pulses were applied for 5 s to potentials from −10 to +50 mV in 10-mV steps from a holding potential of −40 mV; the test pulse was followed by a repolarizing step to −40 mV to observe the tail current.

Statistical analysis

Average values are expressed as means ± SEM. When comparing two groups, Student's *t* test was performed. One sample *t* test was used to compare an effect to a hypothetical effect of 0. The one sample *t* test is a built-in statistical hypothesis test in the GraphPad Prism software, used to determine whether the mean calculated from sample data collected from a single group is different from a designated value specified by the researcher. When comparing multiple groups, a one-way ANOVA was performed, followed by Dunnett's multiple comparisons test when comparing to a single reference group. For cardiomyocyte experiments, two-way ANOVA followed by Bonferroni post hoc analysis was used. A *P* value of <0.05 was considered statistically significant. All statistical analyses were carried out in GraphPad Prism 8.

Supplementary Materials

This PDF file includes:

Figs. S1 to S6
Tables S1 to S6
References

View/request a protocol for this paper from *Bio-protocol*.

REFERENCES AND NOTES

1. J. M. Nerbonne, R. S. Kass, Molecular physiology of cardiac repolarization. *Physiol. Rev.* **85**, 1205–1253 (2005).
2. P. L. Hedley, P. Jorgensen, S. Schlamowitz, R. Wangari, J. Moolman-Smook, P. A. Brink, J. K. Kanters, V. A. Corfield, M. Christiansen, The genetic basis of long QT and short QT syndromes: A mutation update. *Hum. Mutat.* **30**, 1486–1511 (2009).
3. D. M. Roden, Clinical practice. Long-QT syndrome. *N. Engl. J. Med.* **358**, 169–176 (2008).
4. P. J. Schwartz, M. Stramba-Badiale, L. Crotti, M. Pedrazzini, A. Besana, G. Bosi, F. Gabbarini, K. Goulene, R. Insolia, S. Mannarino, F. Mosca, L. Nespoli, A. Rimini, E. Rosati, P. Salice, C. Spazzolini, Prevalence of the congenital long-QT syndrome. *Circulation* **120**, 1761–1767 (2009).
5. N. Guettler, K. Rajappan, E. Nicol, The impact of age on long QT syndrome. *Aging (Albany NY)* **11**, 11795–11796 (2019).
6. M. L. Ponte, G. A. Keller, G. Di Girolamo, Mechanisms of drug induced QT interval prolongation. *Curr. Drug Saf.* **5**, 44–53 (2010).
7. N. El-Sherif, G. Turitto, M. Boutjdir, Acquired long QT syndrome and electrophysiology of torsade de pointes. *Arrhythm Electrophysiol. Rev.* **8**, 122–130 (2019).
8. K. E. Odening, G. Koren, How do sex hormones modify arrhythmogenesis in long QT syndrome? Sex hormone effects on arrhythmogenic substrate and triggered activity. *Heart Rhythm* **11**, 2107–2115 (2014).
9. M. P. Thomas, B. V. L. Potter, The structural biology of oestrogen metabolism. *J. Steroid Biochem. Mol. Biol.* **137**, 27–49 (2013).
10. D. L. Wolbrette, Risk of proarrhythmia with class III antiarrhythmic agents: Sex-based differences and other issues. *Am. J. Cardiol.* **91**, 39D–44D (2003).
11. I. Rodriguez, M. J. Kilborn, X. K. Liu, J. C. Pezzullo, R. L. Woosley, Drug-induced QT prolongation in women during the menstrual cycle. *JAMA* **285**, 1322–1326 (2001).
12. A. J. Sauer, A. J. Moss, S. McNitt, D. R. Peterson, W. Zareba, J. L. Robinson, M. Qi, I. Goldenberg, J. B. Hobbs, M. J. Ackerman, J. Benhorin, W. J. Hall, E. S. Kaufman, E. H. Locati, C. Napolitano, S. G. Priori, P. J. Schwartz, J. A. Towbin, G. M. Vincent, L. Zhang, Long QT syndrome in adults. *J. Am. Coll. Cardiol.* **49**, 329–337 (2007).
13. M. C. Sanguinetti, M. E. Curran, A. Zou, J. Shen, P. S. Spector, D. L. Atkinson, M. T. Keating, Coassembly of K(V)LQT1 and minK (IsK) proteins to form cardiac I(Ks) potassium channel. *Nature* **384**, 80–83 (1996).
14. J. Barhanin, F. Lesage, E. Guillemare, M. Fink, M. Lazdunski, G. Romey, K(V)LQT1 and IsK (minK) proteins associate to form the I(Ks) cardiac potassium current. *Nature* **384**, 78–80 (1996).
15. M. Wang, R. S. Kass, Stoichiometry of the slow I(ks) potassium channel in human embryonic stem cell-derived myocytes. *Pediatr. Cardiol.* **33**, 938–942 (2012).
16. M. D. Drici, T. R. Burklow, V. Haridasse, R. I. Glazer, R. L. Woosley, Sex hormones prolong the QT interval and downregulate potassium channel expression in the rabbit heart. *Circulation* **94**, 1471–1474 (1996).
17. P. Hou, J. Eldstrom, J. Shi, L. Zhong, K. McFarland, Y. Gao, D. Fedida, J. Cui, Inactivation of KCNQ1 potassium channels reveals dynamic coupling between voltage sensing and pore opening. *Nat. Commun.* **8**, 1730 (2017).
18. C. Kang, C. Tian, F. D. Sonnichsen, J. A. Smith, J. Meiler, A. L. George Jr., C. G. Vanoye, H. J. Kim, C. R. Sanders, Structure of KCNE1 and implications for how it modulates the KCNQ1 potassium channel. *Biochemistry* **47**, 7999–8006 (2008).
19. N. Fuentes, P. Silveyra, Estrogen receptor signaling mechanisms. *Adv. Protein Chem. Struct. Biol.* **116**, 135–170 (2019).
20. R. Losel, M. Wehling, Nongenomic actions of steroid hormones. *Nat. Rev. Mol. Cell Biol.* **4**, 46–55 (2003).
21. A. W. Norman, M. T. Mizwicki, D. P. G. Norman, Steroid-hormone rapid actions, membrane receptors and a conformational ensemble model. *Nat. Rev. Drug Discov.* **3**, 27–41 (2004).
22. A. Aranda, A. Pascual, Nuclear hormone receptors and gene expression. *Physiol. Rev.* **81**, 1269–1304 (2001).
23. D. P. Edwards, Regulation of signal transduction pathways by estrogen and progesterone. *Annu. Rev. Physiol.* **67**, 335–376 (2005).
24. Y.-J. Lai, D. Yu, J. H. Zhang, G.-J. Chen, Cooperation of genomic and rapid nongenomic actions of estrogens in synaptic plasticity. *Mol. Neurobiol.* **54**, 4113–4126 (2017).

25. R. Rapetti-Mauss, F. O'Mahony, F. V. Sepulveda, V. Urbach, B. J. Harvey, Oestrogen promotes KCNQ1 potassium channel endocytosis and postendocytic trafficking in colonic epithelium. *J. Physiol.* **591**, 2813–2831 (2013).
26. B. M. Kroncke, W. D. Van Horn, J. Smith, C. Kang, R. C. Welch, Y. Song, D. P. Nannemann, K. C. Taylor, N. J. Sisco, A. L. George Jr., J. Meiler, C. G. Vanoye, C. R. Sanders, Structural basis for KCNE3 modulation of potassium recycling in epithelia. *Sci. Adv.* **2**, e1501228 (2016).
27. R. Alzamora, F. O'Mahony, V. Bustos, R. Rapetti-Mauss, V. Urbach, L. P. Cid, F. V. Sepulveda, B. J. Harvey, Sexual dimorphism and oestrogen regulation of KCNE3 expression modulates the functional properties of KCNQ1 K^+ channels. *J. Physiol.* **589**, 5091–5107 (2011).
28. H. A. Hassan, S. Mentone, L. P. Karniski, V. M. Rajendran, P. S. Aronson, Regulation of anion exchanger Slc26a6 by protein kinase C. *Am. J. Physiol. Cell Physiol.* **292**, C1485–C1492 (2007).
29. J. M. Rocheleau, S. D. Gage, W. R. Kobertz, Secondary structure of a KCNE cytoplasmic domain. *J. Gen. Physiol.* **128**, 721–729 (2006).
30. I. Splawski, M. Tristani-Firouzi, M. H. Lehmann, M. C. Sanguinetti, M. T. Keating, Mutations in the hminK gene cause long QT syndrome and suppress IKs function. *Nat. Genet.* **17**, 338–340 (1997).
31. L.-P. Lai, Y.-N. Su, F.-T. Chiang, J.-M. Juang, Y.-B. Liu, Y.-L. Ho, W.-J. Chen, S.-J. Yeh, C.-C. Wang, Y.-L. Ko, T.-J. Wu, K.-C. Ueng, M.-H. Lei, H.-M. Tsao, S.-A. Chen, T.-K. Lin, M.-H. Wu, H.-M. Lo, S. K. S. Huang, J.-L. Lin, Denaturing high-performance liquid chromatography screening of the long QT syndrome-related cardiac sodium and potassium channel genes and identification of novel mutations and single nucleotide polymorphisms. *J. Hum. Genet.* **50**, 490–496 (2005).
32. M. J. Ackerman, D. J. Tester, G. S. Jones, M. L. Will, C. R. Burrow, M. E. Curran, Ethnic differences in cardiac potassium channel variants: Implications for genetic susceptibility to sudden cardiac death and genetic testing for congenital long QT syndrome. *Mayo Clin. Proc.* **78**, 1479–1487 (2003).
33. J. M. Nerbonne, Molecular basis of functional voltage-gated K^+ channel diversity in the mammalian myocardium. *J. Physiol.* **525**, 285–298 (2000).
34. H.-X. B. Zhang, L. Heckman, Z. Niday, S. Jo, A. Fujita, J. Shim, R. Pandey, H. Al Jandal, S. Jayakar, L. B. Barrett, J. Smith, C. J. Woolf, B. P. Bean, Cannabidiol activates neuronal Kv7 channels. *eLife* **11**, e73246 (2022).
35. J. C. Eldridge, In vitro receptor binding assays. *Issues Toxicol.* **19**, 289–310 (2014).
36. S. Waldegger, U. Lang, T. Herzer, H. Suessbrich, K. Binder, A. Lepple-Wienhues, U. Nagl, M. Paulmichl, H. B. Franz, L. Kiesl, F. Lang, A. E. Busch, Inhibition of minK protein induced K+ channels in Xenopus oocytes by estrogens. *Naunyn Schmiedebergs Arch. Pharmacol.* **354**, 698–702 (1996).
37. C. Moller, R. Netzer, Effects of estradiol on cardiac ion channel currents. *Eur. J. Pharmacol.* **532**, 44–49 (2006).
38. F. Berger, U. Borchard, D. Hafner, I. Putz, T. M. Weis, Effects of 17beta-estradiol on action potentials and ionic currents in male rat ventricular myocytes. *Naunyn Schmiedebergs Arch. Pharmacol.* **356**, 788–796 (1997).
39. S. Tanabe, T. Hata, M. Hiraoka, Effects of estrogen on action potential and membrane currents in guinea pig ventricular myocytes. *Am. J. Physiol.* **277**, H826–H833 (1999).
40. L.-M. Kow, D. W. Pfaff, Rapid estrogen actions on ion channels: A survey in search for mechanisms. *Steroids* **111**, 46–53 (2016).
41. M. Druzin, E. Malinina, O. Grimsholm, S. Johansson, Mechanism of estradiol-induced block of voltage-gated K+ currents in rat medial preoptic neurons. *PLOS ONE* **6**, e20213 (2011).
42. S. T. Granados, K. Castillo, F. Bravo-Moraga, R. V. Sepulveda, W. Carrasquel-Ursulaez, M. Rojas, E. Carmona, Y. Lorenzo-Ceballos, F. Gonzalez-Nilo, C. Gonzalez, R. Latorre, Y. P. Torres, The molecular nature of the 17β-estradiol binding site in the voltage- and Ca^{2+}-activated K^+ (BK) channel β1 subunit. *Sci. Rep.* **9**, 9965 (2019).
43. P.-C. Yang, L. L. Perissinotti, F. Lopez-Redondo, Y. Wang, K. R. DeMarco, M.-T. Jeng, I. Vorobyov, R. D. Harvey, J. Kurokawa, S. Y. Noskov, C. E. Clancy, A multiscale computational modelling approach predicts mechanisms of female sex risk in the setting of arousal-induced arrhythmias. *J. Physiol.* **595**, 4695–4723 (2017).
44. A. Lvov, S. D. Gage, V. M. Berrios, W. R. Kobertz, Identification of a protein-protein interaction between KCNE1 and the activation gate machinery of KCNQ1. *J. Gen. Physiol.* **135**, 607–618 (2010).
45. J. Chen, Z. Liu, J. Creagh, R. Zheng, T. V. McDonald, Physical and functional interaction sites in cytoplasmic domains of KCNQ1 and KCNE1 channel subunits. *Am. J. Physiol. Heart Circ. Physiol.* **318**, H212–H222 (2020).
46. G. Kuenze, C. G. Vanoye, R. R. Desai, S. Adusumilli, K. R. Brewer, H. Woods, E. F. McDonald, C. R. Sanders, A. L. George Jr., J. Meiler, Allosteric mechanism for KCNE1 modulation of KCNQ1 potassium channel activation. *eLife* **9**, e57680 (2020).
47. I. Galleano, H. Harms, K. Choudhury, K. Khoo, L. Delemotte, S. A. Pless, Functional cross-talk between phosphorylation and disease-causing mutations in the cardiac sodium channel $Na_v1.5$. *Proc. Natl. Acad. Sci. U.S.A.* **118**, e2025320118 (2021).
48. Y. Li, M. A. Zaydman, D. Wu, J. Shi, M. Guan, B. Virgin-Downey, J. Cui, KCNE1 enhances phosphatidylinositol 4,5-bisphosphate (PIP2) sensitivity of IKs to modulate channel activity. *Proc. Natl. Acad. Sci. U.S.A.* **108**, 9095–9100 (2011).
49. P. W. Kang, A. M. Westerlund, J. Shi, K. M. White, A. K. Dou, A. H. Cui, J. R. Silva, L. Delemotte, J. Cui, Calmodulin acts as a state-dependent switch to control a cardiac potassium channel opening. *Sci. Adv.* **6**, eabd6798 (2020).
50. M. Bjelic, W. Zareba, D. R. Peterson, A. Younis, M. K. Aktas, D. T. Huang, S. Rosero, K. Cutter, S. McNitt, X. Xia, B. D. MacKecknie, R. Horn, N. Sotoodehnia, P. J. Kudenchuk, T. D. Rea, D. E. Arking, A. A. M. Wilde, W. Shimizu, M. J. Ackerman, I. Goldenberg, Sex hormones and repolarization dynamics during the menstrual cycle in women with congenital long QT syndrome. *Heart Rhythm* **19**, 1532–1540 (2022).
51. M. Kim, D. Ye, C. S. John Kim, W. Zhou, D. J. Tester, J. R. Giudicessi, M. J. Ackerman, Development of a patient-specific p.D85N-potassium voltage-gated channel subfamily E member 1-induced pluripotent stem cell-derived cardiomyocyte model for drug-induced long QT syndrome. *Circ. Genom. Precis. Med.* **14**, e003234 (2021).
52. J. Kurokawa, M. Tamagawa, N. Harada, S.-I. Honda, C.-X. Bai, H. Nakaya, T. Furukawa, Acute effects of oestrogen on the guinea pig and human IKr channels and drug-induced prolongation of cardiac repolarization. *J. Physiol.* **586**, 2961–2973 (2008).
53. R. R. Kauthale, S. S. Dadarkar, R. Husain, V. V. Karande, M. M. Gatne, Assessment of temperature-induced hERG channel blockade variation by drugs. *J. Appl. Toxicol.* **35**, 799–805 (2015).
54. F. Ando, A. Kuruma, S. Kawano, Synergic effects of β-estradiol and erythromycin on hERG currents. *J. Membr. Biol.* **241**, 31–38 (2011).
55. S. P. Davies, H. Reddy, M. Caivano, P. Cohen, Specificity and mechanism of action of some commonly used protein kinase inhibitors. *Biochem. J.* **351**, 95–105 (2000).
56. H. Yu, Z. Lin, M. E. Mattmann, B. Zou, C. Terrenoire, H. Zhang, M. Wu, O. B. McManus, R. S. Kass, C. W. Lindsley, C. R. Hopkins, M. Li, Dynamic subunit stoichiometry confers a progressive continuum of pharmacological sensitivity by KCNQ potassium channels. *Proc. Natl. Acad. Sci. U.S.A.* **110**, 8732–8737 (2013).
57. Y. Wang, J. Eldstrom, D. Fedida, Gating and regulation of KCNQ1 and KCNQ1 + KCNE1 channel complexes. *Front. Physiol.* **11**, 504 (2020).
58. X. Wu, H. P. Larsson, Insights into cardiac IKs (KCNQ1/KCNE1) channels regulation. *Int. J. Mol. Sci.* **21**, 9440 (2020).
59. J. E. Larsson, H. P. Larsson, S. I. Liin, KCNE1 tunes the sensitivity of KV7.1 to polyunsaturated fatty acids by moving turret residues close to the binding site. *eLife* **7**, e37257 (2018).
60. S. I. Liin, M. Silvera Ejneby, R. Barro-Soria, M. A. Skarsfeldt, J. E. Larsson, F. Starck Harlin, T. Parkkari, B. H. Bentzen, N. Schmitt, H. P. Larsson, F. Elinder, Polyunsaturated fatty acid analogs act antiarrhythmically on the cardiac IKs channel. *Proc. Natl. Acad. Sci. U.S.A.* **112**, 5714–5719 (2015).
61. T. O'Hara, L. Virag, A. Varro, Y. Rudy, Simulation of the undiseased human cardiac ventricular action potential: Model formulation and experimental validation. *PLoS Comput. Biol.* **7**, e1002061 (2011).
62. V. Piacentino 3rd, C. R. Weber, X. Chen, J. Weisser-Thomas, K. B. Margulies, D. M. Bers, S. R. Houser, Cellular basis of abnormal calcium transients of failing human ventricular myocytes. *Circ. Res.* **92**, 651–658 (2003).
63. S. I. Liin, J. E. Larsson, R. Barro-Soria, B. H. Bentzen, H. P. Larsson, Fatty acid analogue N-arachidonoyl taurine restores function of I_{Ks} channels with diverse long QT mutations. *eLife* **5**, e20272 (2016).
64. G. Q. Xiao, Y. Qu, Z. Q. Sun, D. Mochly-Rosen, M. Boutjdir, Evidence for functional role of epsilonPKC isozyme in the regulation of cardiac Na(+) channels. *Am. J. Physiol. Cell Physiol.* **281**, C1477–C1486 (2001).
65. K. E. Odening, I. Bodi, G. Franke, R. Rieke, A. Ryan de Medeiros, S. Perez-Feliz, H. Furniss, L. Mettke, K. Michaelides, C. N. Lang, J. Steinfurt, N. D. Pantulu, D. Ziupa, M. Menza, M. Zehender, H. Bugger, R. Peyronnet, J. C. Behrends, Z. Doleschall, A. Zur Hausen, C. Bode, G. Jolivet, M. Brunner, Transgenic short-QT syndrome 1 rabbits mimic the human disease phenotype with QT/action potential duration shortening in the atria and ventricles and increased ventricular tachycardia/ventricular fibrillation inducibility. *Eur. Heart J.* **40**, 842–853 (2019).
66. H.-S. Na, H.-P. Park, C.-S. Kim, S.-H. Do, Z. Zuo, C.-S. Kim, 17β-Estradiol attenuates the activity of the glutamate transporter type 3 expressed in Xenopus oocytes. *Eur. J. Pharmacol.* **676**, 20–25 (2012).
67. C. Peyton, P. Thomas, Involvement of epidermal growth factor receptor signaling in estrogen inhibition of oocyte maturation mediated through the G protein-coupled estrogen receptor (Gper) in zebrafish (Danio rerio). *Biol. Reprod.* **85**, 42–50 (2011).
68. C. M. B. Lopes, J. I. Remon, A. Matavel, J. L. Sui, I. Keselman, E. Medei, Y. Shen, A. Rosenhouse-Dantsker, T. Rohacs, D. E. Logothetis, Protein kinase A modulates PLC-dependent regulation and PIP2-sensitivity of K+ channels. *Channels (Austin)* **1**, 124–134 (2007).
69. S. Doolen, N. R. Zahniser, Conventional protein kinase C isoforms regulate human dopamine transporter activity in Xenopus oocytes. *FEBS Lett.* **516**, 187–190 (2002).

70. S. Kathofer, K. Rockl, W. Zhang, D. Thomas, H. Katus, J. Kiehn, V. Kreye, W. Schoels, C. Karle, Human beta(3)-adrenoreceptors couple to KvLQT1/MinK potassium channels in Xenopus oocytes via protein kinase C phosphorylation of the KvLQT1 protein. *Naunyn Schmiedebergs Arch. Pharmacol.* **368**, 119–126 (2003).
71. I. Zaltsman, H. Grimberg, M. Lupu-Meiri, L. Lifschitz, Y. Oron, Rapid desensitization of the TRH receptor and persistent desensitization of its constitutively active mutant. *Br. J. Pharmacol.* **130**, 315–320 (2000).
72. E. P. Scholz, F. Welke, N. Joss, C. Seyler, W. Zhang, D. Scherer, M. Volkers, R. Bloehs, D. Thomas, H. A. Katus, C. A. Karle, E. Zitron, Central role of PKCα in isoenzyme-selective regulation of cardiac transient outward current Ito and Kv4.3 channels. *J. Mol. Cell. Cardiol.* **51**, 722–729 (2011).
73. C. Braun, X. X. Parks, H. Qudsi, C. M. Lopes, PKCβII specifically regulates KCNQ1/KCNE1 channel membrane localization. *J. Mol. Cell. Cardiol.* **138**, 283–290 (2020).
74. R. Efendiev, A. M. Bertorello, C. H. Pedemonte, PKC-beta and PKC-zeta mediate opposing effects on proximal tubule Na+,K+-ATPase activity. *FEBS Lett.* **456**, 45–48 (1999).
75. X. Gou, T. Hu, Y. Gou, C. Li, M. Yi, M. Jia, Specific protein kinase C isoform exerts chronic inhibition on the slowly activating delayed-rectifier potassium current by affecting channel trafficking. *Channels (Austin)* **15**, 262–272 (2021).
76. J.-T. Pougnet, E. Toulme, A. Martinez, D. Choquet, E. Hosy, E. Boue-Grabot, ATP P2X receptors downregulate AMPA receptor trafficking and postsynaptic efficacy in hippocampal neurons. *Neuron* **83**, 417–430 (2014).
77. K. Vijayaragavan, M. Boutjdir, M. Chahine, Modulation of Nav1.7 and Nav1.8 peripheral nerve sodium channels by protein kinase A and protein kinase C. *J. Neurophysiol.* **91**, 1556–1569 (2004).
78. Z. Han, M. B. Wax, R. V. Patil, Regulation of aquaporin-4 water channels by phorbol ester-dependent protein phosphorylation. *J. Biol. Chem.* **273**, 6001–6004 (1998).

Acknowledgments: We thank E. Nilsson for contributions to experiments during her time as visiting scholar. We also wish to thank S. Nimani and N. Alerni for help in isolating the rabbit cardiomyocytes used in this study. **Funding:** This work was funded by a grant from the European Research Council under the European Union's Horizon 2020 research and innovation program (grant agreement no. 850622) to S.I.L. **Author contributions:** L.-M.E. and J.N. contributed to study design, collection of data, data analysis, and writing the manuscript. A.H. contributed to collection of data, data analysis, and writing the manuscript. L.G. contributed to collection of data in rabbit cardiomyocytes, data analysis, and writing the manuscript. H.G. contributed to study design and writing the manuscript. K.E.O. supervised the rabbit cardiomyocyte experiments and contributed to data interpretation and writing the manuscript. S.I.L. contributed to study design, collection of data, data analysis, writing the manuscript, and funding acquisition. **Competing interests:** The authors declare that they have no competing interests. **Data and materials availability:** All data needed to evaluate the conclusions in the paper are present in the paper and/or the Supplementary Materials.

Submitted 2 September 2022
Accepted 13 February 2023
Published 15 March 2023
10.1126/sciadv.ade7109